ZJUT-EIFD: A Synchronously Collected External and Internal Fingerprint Database

Haohao Sun, Haixia Wang, *Member, IEEE*, Yilong Zhang, *Member, IEEE*, Ronghua Liang, *Senior Member, IEEE*, Peng Chen, *Member, IEEE*, and Jianjiang Feng, *Member, IEEE*

***Abstract*—External fingerprints (EFs) based only on epidermal information are vulnerable to spoofing attacks and non-ideal skin conditions. To solve such shortcomings, internal fingerprints (IFs) collected using optical coherence tomography (OCT) have been proposed and widely researched. However, the development of IF is limited by the lack of in-depth researches on the IF and the EF-IF interoperability, which is partially caused by the lack of public OCT database. The obvious gap in the applications of EF and IF recognition motivated us to design and publish a comprehensive fingerprint database containing both traditional EFs and OCT IFs, denoted as ZJUT-EIFD. To the best of our knowledge, ZJUT-EIFD is the first public database that combines OCT and total internal reflection (TIR) via synchronous acquisition, with 399 different fingers from 60 subjects. In this article, the composition of the database, the quality of EFs and IFs, and the verification performance of different types of fingerprints were detailed. In addition, potential application directions of ZJUT-EIFD were demonstrated. ZJUT-EIFD can serve benchmarks and interoperability tests for EF-IF research, which will promote the research and development of EF and IF.**

***Index Terms*—Biometrics, fingerprint database, total internal reflection, optical coherence tomography, fingerprint recognition.**

Fig. 1. Examples of spoofing artifact and fingerprints obtained under poor skin conditions.

I Introduction

With the continuous development of information technology, biometric identification has played a crucial part in security-related applications, such as national defense, financial security, intelligent human–computer interaction, etc [1], [2], [3]. Within various biometrics, fingerprint has become one of the most widely used identification features due to its uniqueness, permanence, simplicity, reliability, and accuracy [4], [5], [6], [7], where the former two are the basis of fingerprint identification [8]. For uniqueness, it has been generally believed that no two individuals (including monozygotic twins) have exactly the same fingerprints [9], [10]. For permanence, it has also been claimed that even if fingerprints temporarily change due to minor cuts and bruises on the skin, the original ridge pattern reverts after the finger heals except for a significant injury that creates a permanent scar [7].

However, the development of current mainstream fingerprint technology is limited by capturing only skin surface information. Commercial off-the-shelf automatic fingerprint identification systems (AFIS), which are mainly based on the protrusions and depressions of the stratum corneum (the outermost layer of the epidermis), suffer from spoofing attacks and unstable fingerprint quality. Taking fingerprint images by total internal reflection (TIR) as examples, as shown in Fig. 1, the anti-spoofing and identification performances drop rapidly under the influence of various spoofing attacks and poor skin conditions (e.g., dirt, dryness, sweat, scars, wounds, warts, attachments, wrinkles, aging and creases, etc.) [11], [12], [13], [14], [15], [16].

Fortunately, with the development of optics, fiber optics, and laser technology, optical coherence tomography (OCT) has become an indispensable tool in biomedical and biometric imaging [17], [18]. The application of internal fingerprint (IF) obtained by OCT to fingerprint identification has become an active research area to reduce the defects of external fingerprint

Manuscript received 2 January 2023; revised 3 October 2023; accepted 4 November 2023. Date of publication 28 November 2023; date of current version 6 March 2024. This work was supported in part by the National Natural Science Foundation of China under Grants 61976189, 62276236, and U1909203, and in part by Zhejiang Provincial Leading Innovation and Entrepreneurship Team under Grant 2021R01002. Recommended for acceptance by W. Scheirer. *(Corresponding author: Haixia Wang.)*

Haohao Sun, Haixia Wang, Yilong Zhang, Ronghua Liang, and Peng Chen are with the College of Computer Science & Technology, Zhejiang University of Technology, Hangzhou 310023, China (e-mail: hhsun@zjut.edu.cn; hxwang@zjut.edu.cn; zhangyilong@zjut.edu.cn; rhliang@zjut.edu.cn; chenpeng@zjut.edu.cn).

Jianjiang Feng is with the Department of Automation, Tsinghua University, Beijing 100084, China, and also with the Beijing National Research Center for Information Science and Technology, Tsinghua University, Beijing 100084, China (e-mail: jfeng@tsinghua.edu.cn).

ZJUT-EIFD is available at https://github.com/ZJUT-ERCISS-home/ZJUT-EIFD/

Digital Object Identifier 10.1109/TPAMI.2023.3334760

(EF) [19], [20], [21], [22]. Bossen et al. conducted matching experiments on the IFs extracted from OCT cross-sectional images (called B-scan images, and the lines formed in the depth direction are called A-lines) and found that the IFs can be used for accurate and reliable fingerprint recognition [23]. Aum et al. intuitively compared the quality between IFs and EFs. It is found that the OCT IFs can effectively resist the poor quality of EFs under the conditions of wetness, attachment, and damage [21]. Yu et al. obtained clear IFs and subcutaneous sweat pore images by enface imaging and contrast-enhanced method [24]. Liu et al. realized the successful detection of multiple types of spoofing attacks by peak features (called depth-double-peak feature and sub-single-peak feature) [25] and neural networks [26]. Yu et al. used neural networks to complete the style conversion between OCT fingerprints and TIR fingerprints, and realized the meticulous registration of fingerprints from different collection devices [27]. Ding et al. introduced deep learning into the OCT fingerprint reconstruction, and demonstrated that IF has better identification performance than EF when the hand condition is poor [28]. These studies have proved the application prospects of IF in recognition.

The development of IF in real-world applications is limited by the lack of in-depth research on IF and large OCT databases. IF is considered as a supplement to traditional EF due to the following reasons: 1) The fingerprint equipment used to enroll a user's fingerprint image at one location (e.g., conventional EF reader) may not be the same equipment used later to identify or verify the same individual at another location (e.g., OCT IF equipment). 2) The cost of re-enrolling all users by OCT IF equipment could be prohibitively high [15], [29], [30]. These situations underscore the necessity of studying the EF-IF interoperability before local deployment or trial use of OCT AFISs. However, EF-IF interoperability remains a research area far from maturity. Evaluating potential EF-IF interoperability exhaustively and objectively is limited by the lack of data support, which restricts the application of IF in real scenarios.

The obvious gap in the application of EF-IF identification motivated us to design and publish a comprehensive fingerprint database containing both traditional EFs and OCT IFs, denoted as ZJUT-EIFD. It is inspired and acquired by our recent work [31], a synchronous fingerprint acquisition system. ZJUT-EIFD aims to provide benchmarks and interoperability tests for EF-IF research. As far as we know, this is the first public fingerprint database that contains both traditional EFs and OCT IFs collected simultaneously. The synchronous acquisition indicates there is only minimal distortion between the paired fingerprints. Such an advantage gives the proposed database broad prospects for the study of fingerprint interoperability between EFs and IFs.

More concisely, the contributions of this research are:

1) To the best of our knowledge, ZJUT-EIFD is the first public fingerprint database that combines synchronous OCT and TIR acquisitions.
2) ZJUT-EIFD composition is comprehensive. It contains not only the source data of TIR and OCT, but also the processed TIR and OCT fingerprints whose resolutions are normalized to 500 dpi. The source data of OCT consists of high-resolution fingertip cross-sectional images, which can be used as raw data for OCT fingerprint reconstruction and anti-spoofing research.
3) Fingerprints of various types in ZJUT-EIFD are evaluated and discussed in detail. A thorough evaluation of the recognition capabilities and the interoperability of IFs and traditional EFs is conducted using both conventional matcher and deep learning-based matcher. The application potential of IF is demonstrated.

The remaining part of this article is organized as follows. Related works of the OCT fingerprint researches and existing fingerprint databases are presented in Section II. Then, the design of the ZJUT-EIFD is detailed in Section III. The data in ZJUT-EIFD are demonstrated in Section IV. The evaluation of EFs and IFs on the ZJUT-EIFD are presented in Section V. In Section VI, discussions concerning the future research directions of ZJUT-EIFD are carried out. Finally, conclusions are drawn in Section VII.

II Related Works

A. Acquisition of EF and IF

The wide application of EF is inseparable from the diversity of EF acquisition technologies. The most widely used in the early days was ink-pressed fingerprints [7]. As time advances, different techniques have been developed for EF acquisition. Tartagni et al. used silicon-based micro-capacitor plates to acquire EFs [32]. The solid-state sensor requires neither optical components nor an external image sensor. Bahuguna et al. used a holographic prism to obtain TIR EF, which not only guaranteed the image quality but also reduced the volume of optical components [33]. Parizale et al. used 5 cameras and obtained 3D EF based on stereo vision [34]. Liu et al. used 3 cameras to achieve multi-view EF acquisition and mosaicking [35]. Kumar et al. used a multi-light source single camera and Photometric Stereo to achieve 3D EF acquisition and reconstruction [36]. Lu et al. used capacitive micromachined ultrasonic transducers and obtained ultrasonic EF at 254 dpi resolution [37]. Wang et al. introduced an EF acquisition technique using structured light illumination to acquire high-resolution 3D EF using a single camera [38]. Engelsma et al. combined direct imaging and TIR technology into a device called RaspiReader, which can simultaneously obtain these two types of EFs [39]. Grosz et al. used mobile phones to obtain finger photos. They proposed a contact to contactless fingerprint matching method and verified the cross-database performance under contactless and contact fingerprints [40]. However, all these methods for fingerprint acquisition only acquire finger surface information. The spread of EF applications is still limited by the uncontrollable hand conditions and the diversity of spoofing materials [41].

Unlike EF acquisition devices, IF acquisition is realized mainly using OCT to acquire images of the internal structure of the skin at a depth of mm. OCT techniques can be divided into B-scan-based and C-scan-based methods [18]. For B-scan-based methods, the skin structure is composed of a series of cross-sectional images through the lateral scanning of the light beam. As the beam finally scans all positions, the OCT 3D volume data of the internal finger structure is

formed. This technology includes two different OCT types: time-domain OCT (TD-OCT) and Fourier/frequency-domain OCT (FD-OCT). FD-OCT can be divided into spectral domain OCT (SD-OCT) and swept source OCT (SS-OCT). Cheng et al. used autocorrelation analysis to verify the ability of TD-OCT to resist artificial fingerprints [19]. Alex et al. built multiple FD-OCT systems using light sources of different wavelengths and classified the internal physiology of the skin in detail [42]. For the C-scan-based method, it is mainly achieved by full-field OCT (FF-OCT). An en-face image of a certain depth can be obtained by single acquisition of FF-OCT. The formation of volume data requires scanning of all depths. Auksorius et al. used FF-OCT to image the finger and compared the difference between the IFs of FF-OCT and EFs of TIR [43].

Compared with traditional fingerprint collection devices that can directly obtain EFs for recognition, the volume data collected by OCT is difficult to use for direct matching due to problems such as large redundant data and high speckle noise. To be more compatible with existing fingerprint matching algorithms, extraction algorithms that reconstruct OCT fingerprints from OCT volume data are required.

B. OCT Fingerprint Reconstruction

The purpose of the OCT fingerprint reconstruction is to quickly and accurately extract fingerprint information from the 3D structure. According to the different extraction depths in the internal structure of the fingertip, OCT fingerprints can be divided into EFs and IFs. The EFs are mainly formed by the protrusions and depressions of the stratum corneum. The IFs mainly come from the boundary between the viable epidermis and the stratum corneum. In the application of OCT fingertip imaging, past studies have shown that the IF pattern is consistent with the epidermis [21]. The IFs extracted from the viable epidermis junction are not easily damaged and forged, thereby becoming powerful complements of EFs [28], [44], [45].

With the manifestation of the superiority of IFs, a variety of reconstruction methods have been proposed to generate better-quality OCT fingerprints. These methods can be roughly divided into two categories: en-face-based methods and contour-based methods.

In the en-face-based methods, FF-OCT can directly obtain the IF of fixed depth. Raja et al. proposed a quality metric-based framework to fuse different fixed-depth IFs directly obtained by FF-OCT [46]. Whether it is TD-OCT or FD-OCT, the IF images are mainly obtained by accumulating and averaging pixels with a fixed depth or manually selected depth range in the B-scan. Liu et al. [47] and Bossen et al. [23] set up different fixed depth regions of OCT volume data for EF, IF, and sweat pore images reconstruction, respectively. Zam et al. extracted IF and sweat pores by manually segmenting the stratum corneum and viable epidermis [48]. After that, the automatic depth detection was applied to enface-based OCT fingerprint generation. Aum et al. used the Sobel operation in the depth direction to locate the edge of the viable epidermis and reconstructed the IF from it [21]. Liu et al. projected all the A-lines in a B-scan image to form a single accumulated A-line profile, called RobustAline [49]. The RobustAline is used to automatically find the projection zone, and the depth pixels are accumulated in this zone to generate IF, EF, and papillary fingerprint. Compared to contour-based methods, enface-based methods generally have a speed advantage because precise contour location of different layers of the skin is not required. However, the accumulation of pixels in depth also means the accumulation of noise and errors, which leads to a decreased fingerprint quality. In response to this defect, Liu et al. proposed a fingerprint fusion method to improve the quality of OCT fingerprints [49].

The aim of the contour-based method is to precisely locate the different layers of the skin structure (mainly stratum corneum and viable epidermis). The reconstructed fingerprint is generated according to the gray information or depth information of the corresponding position in the 3D structure of the finger. The quality of OCT fingerprints generated by the contour-based method depends on the accuracy of contour extraction. Previous methods relied on some image gradient operators or maximum search methods to locate skin layers, such as Findpeaks (Matlab function) [50], Sobel [51], [52], Otsu [53], etc. Later, some clustering methods are applied to segment different skin structures, such as K-means [53], fuzzy C-means [54], hybrid hierarchical clustering [55], etc. Recently, the use of neural networks for fingertip OCT volume data segmentation and reconstruction has been proposed. Wang et al. used 3D U-Net to process OCT volume data and achieved accurate pixel-wise segmentation [56]. Ding et al. proposed a network with the best segmentation performance so far, (called BCL-U Net), which can simultaneously segment the stratum corneum, viable epidermis, and sweat glands [28].

However, these researches on OCT IFs have two major limitations caused by the data used: 1) The self-built OCT databases are not public and the amount of data is limited. Data discrepancies may lead to disagreement in the applicability assessment of these methods; 2) the difference between the OCT IF and the EF collected by traditional devices is not paid enough attention, the interoperability may limit the promotion of OCT fingerprints. These limitations suggest the need for a targeted EF-IF database for objective algorithm evaluation and testing.

C. Fingerprint Database

In recent years, the widespread of fingerprints is benefited from the good performance of recognition algorithms. One of the key points of this success is the availability of fingerprint benchmark databases. Conventional fingerprint databases are well established and widely used. These databases include but are not limited to:

- FVC databases [57], [58], [59], [60]. FVC databases are originated from Fingerprint Verification Competition (FVC). FVC established several common benchmarks, facilitating developers in conducting unambiguous comparative assessments of their respective algorithms. The FVC databases encompass several editions based on the held years, namely FVC2000 [57], FVC2002 [58], FVC2004 [59], and FVC2006 [60], each of which is further subdivided into four distinct subsets denoted as DB1-DB4.

TABLE I
MAIN DIFFERENCES BETWEEN ZJUT-EIFD AND SZU OCTFD

Study	OCT Technology	OCT scanned volume	B-scan number (per instance)	Imaging approach	Database composition
SZU OCTFD[77]	Custom 830nm SD-OCT at 18 KHz A-line rate	15 mm × 15 mm × 1.8 mm	400	OCT	OCT volume (B-scan images)
ZJUT-EIFD	Custom 1310nm SD-OCT at 60 KHz A-line rate	18 mm × 14 mm × 4.64 mm (theoretical depth value)	1400 (white-collar workers) 700 (blue-collar workers)	TIR and OCT Synchronously	TIR image[1] OCT volume (B-scan images) Label of B-scan physiological structure TIR fingerprint image[2] OCT fingerprint image[3]

[1]*The TIR image is the source data captured from the industrial camera.*
[2]*The TIR fingerprint image is the distortion-corrected image of 500 dpi.*
[3]*The OCT fingerprint image is the distortion-corrected image of 500 dpi, the reconstruction method is BCL-U net [28].*

- NIST special databases [61], [62], [63]. The National Institute of Standards and Technology (NIST) offers an array of fingerprint datasets specifically collected to support research and development in the field of fingerprint analysis. Among these, widely utilized datasets encompass NIST SD4 [62] and NIST SD14 [63], among others.
- CASIA-FingerprintV5 [64]. CASIA-FingerprintV5 comprises fingerprints collected from volunteers situated within diverse occupational environments.
- Tsinghua fingerprint database [65], [66], [67]. Tsinghua fingerprint database mainly focuses on distorted fingerprints and latent fingerprints, including: distorted fingerprints [65], latent overlapped fingerprints [66], and simulated overlapped fingerprints [67].
- PolyU fingerprint database [36], [68], [69], [70]. PolyU fingerprint database mainly focuses on non-contact fingerprints, including: contactless 3D fingerprints [36], [68], contactless 2D to contact-based 2D fingerprints [69], and low-resolution fingerprints [70].
- IAB fingerprint databases [71], [72], [73]. The Image Analysis and Biometrics Lab provides diverse fingerprint databases, including finger-selfie database [72], multisensor optical and latent fingerprint database [73], etc.
- SOCOFing [74]. Sokoto Coventry Fingerprint database Dataset (SOCOFing) includes gender labels, finger names, and three different levels of alteration as obliteration, central rotation, and z-cut.
- RidgeBase [75]. RidgeBase is a cross-sensor contactless fingerprint database containing contactless 2D and contact-based 2D fingerprint pairs. The fingerprint pairs were collected using two smartphone cameras and one flatbed contact sensor.

However, limited by the acquisition technologies, the fingerprints in these databases only contain information on the outer epidermis of the fingertips, which are essentially all EFs.

The development of IFs is inseparable from the establishment and disclosure of the OCT fingerprint database. However, there are few IF databases [28], [46], [54], where only the SZU OCT-based fingerprint database (OCTFD) is publicly available [76], [77]. In particular, there are currently only separate conventional EF or OCT databases. The volunteer fingerprints collected in these databases were from different person. Even from the same person, there is a large distortion due to the lack of synchronous acquisition. Unrelated OCT fingerprint and traditional EF databases makes it difficult to perform EF and IF correlation studies. The main differences between our established ZJUT-EIFD and SZU OCT-based fingerprint databases are shown in Table I. Compared to the regular OCT fingerprint dataset, our ZJUT-EIFD is more comprehensive and can be used in combination with traditional fingerprints. The TIR fingerprints and OCT fingerprints provided can be directly used for EF-IF correlation studies.

III ZJUT-EIFD CONSTRUCTION

The data collection of ZJUT-EIFD mainly relies on the TIR and OCT synchronized acquisition system we built previously [31]. This section briefly introduces the acquisition device of ZJUT-EIFD, the method for fingerprint generation, and the database construction.

A. Acquisition Device

1) Device Introduction: Our fingerprint synchronous acquisition system is sketched in Fig. 2, where Fig. 2(a) illustrates the optical schematic of the system and Fig. 2(b) shows the experimental platform. Briefly, the synchronous acquisition system uses a self-designed trapezoidal prism to accomplish the same collection area at the same time. In TIR imaging, the collimated and filtered LED light is totally reflected by the trapezoidal prism. In OCT imaging, a broadband infrared superluminescent diode (SLED) is used as the OCT light source. Light from the SLED is divided into the reference arm and the sample arm by a 50:50 fiber coupler. To obtain 3D tissue volume data on the field of view matching TIR, the probe beam in the sample arm is scanned by a pair of XY current galvanometric mirrors. In the reference arm, another trapezoidal prism is used for dispersion compensation. Light interfered from the sample arm and the reference arm is captured by a spectrometer with an InGaAs line scan camera. The main system parameters of the synchronous acquisition device are shown in Table II [31].

2) Source Data: The source data collected by our synchronization device in each measurement includes a grayscale image

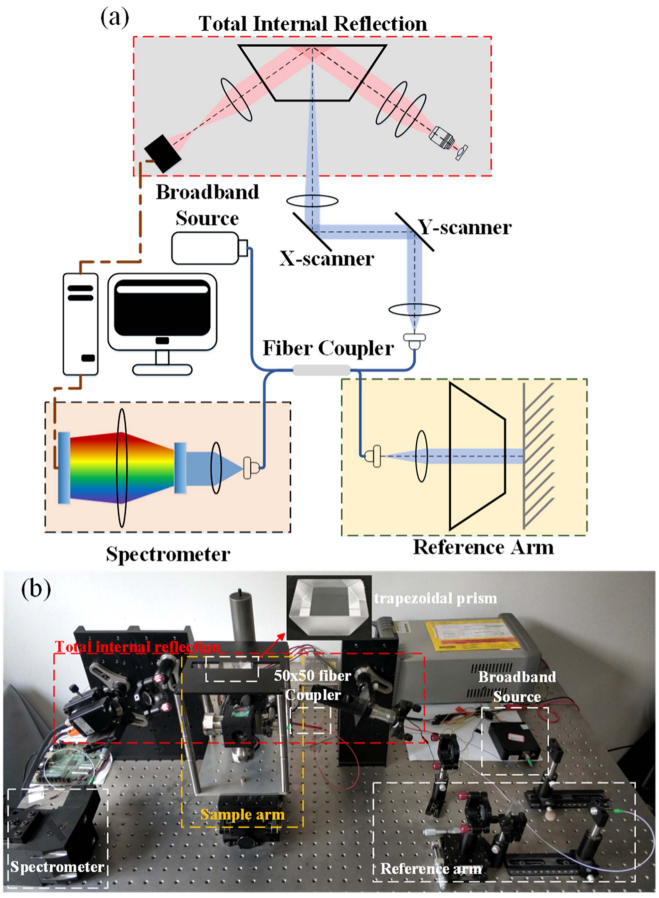

Fig. 2. Experimental setup of fingerprint synchronous acquisition system based on TIR and OCT [31]. (a) Optical schematic; (b) experimental platform.

TABLE II
SYSTEM PARAMETERS OF SYNCHRONOUS ACQUISITION DEVICE

Imaging Method	Specifications
TIR	Image pixel: 1392 × 1040 Image format: Mono 8 bit Measured area: 43 × 16 mm² Acquisition time: < 1s Lateral resolution: 820 dpi Vertical resolution: 1650 dpi
OCT	Light source power: 17mW Center wavelength: 1310nm bandwidth: 85.6nm Coherence length: 13.3μm Axial resolution: 8.82μm in air (~6.3μm in tissue) Scanning lateral resolution: 55.7μm A-line scanning rate: 60kHz Scanning range: 18 × 14 mm² Scan density: 100 spectra per millimeter (typical)

of TIR and a series of grayscale B-scan images of OCT. A presentation of the source data is shown in Fig. 3. As shown in Fig. 3(a), the size of the image captured by TIR is 1392 × 1040. The fingerprint patterns collected by the TIR method are clearly demonstrated. However, due to that the collimated beam is incident obliquely at a certain angle to ensure total reflection during TIR imaging, the resolution compression of the source TIR image on one axis is produced.

As shown in Fig. 3(b), OCT realizes the acquisition of the internal 3D spatial information (X-Y-Z) of the fingertip. Each B-scan image is composed of multiple A-lines in the X direction. A plurality of B-scan images in the Y direction complete a 3D volume (C-scan). The IF can be obtained by extracting information of the viable epidermis from the 3D volume data of the finger.

B. Fingerprint Generation

Considering that the size, distortion, and resolution of source data of TIR and OCT are different, it is necessary to reconstruct and align the fingerprint images in order to study the correlation between IFs and EFs.

1) OCT Fingerprint Reconstruction: The quality and pattern clarity of an OCT fingerprint is directly related to the OCT fingerprint reconstruction method used. To ensure that the reconstruction method has minimal impact on EF-IF correlation studies, the current state-of-the-art contour based method (BCL-U net) [28] is used in our dataset construction.

As shown in Fig. 4, contour extraction results from OCT volume data, including cover glass, stratum corneum junction, and viable epidermis junction, are obtained using BCL-U net. We applied the reconstruction methods of fingerprints in [28] and [56]. All OCT fingerprints corresponding to the source data were generated. The stratum corneum junction is used to generate EF, and the viable epidermis junction is used to generate IF.

For OCT fingerprints based on gray information (*gray*), a line passing through fluctuations of the stratum corneum or viable epidermis junction is used to estimate the fingerprints with maximized intensity variation for ridges and valleys.

For OCT fingerprints based on depth information, there are two different reference planes. The first is the cover glass layer (*depth1*). The second is the polynomial curves fitted from the contours of stratum corneum and viable epidermis junction respectively (*depth2*). The relative depth between the stratum corneum junction or viable epidermis junction and the reference plane forms the fingerprints.

Finally, the fingerprint images are normalized to [0, 255].

2) Fingerprint Distortion Correction and Alignment: Different imaging characteristics lead to different image distortions in the generated TIR and OCT fingerprints. Before fingerprint data collection, we calibrated the distortion parameters for TIR and OCT imaging with the aid of a grid correction plate [31]. The grid correction plate is actually an aluminized plane mirror with a 15 mm × 20 mm grid on the surface, the line spacing is 1 mm, and the line width is 0.01 mm.

As displayed in Fig. 5, the measured landmark point coordinates (distortion coordinates) of the grid correction plate in TIR and OCT imaging and the corresponding real coordinates were obtained. Coordinate mapping was performed using the Thin Plate Spline (TPS) algorithm [78]. The transformation matrix of coordinates is saved and applied to the unaligned TIR and OCT fingerprint images, respectively. Since the current standard fingerprint resolution is 500 dpi and many evaluations are designed

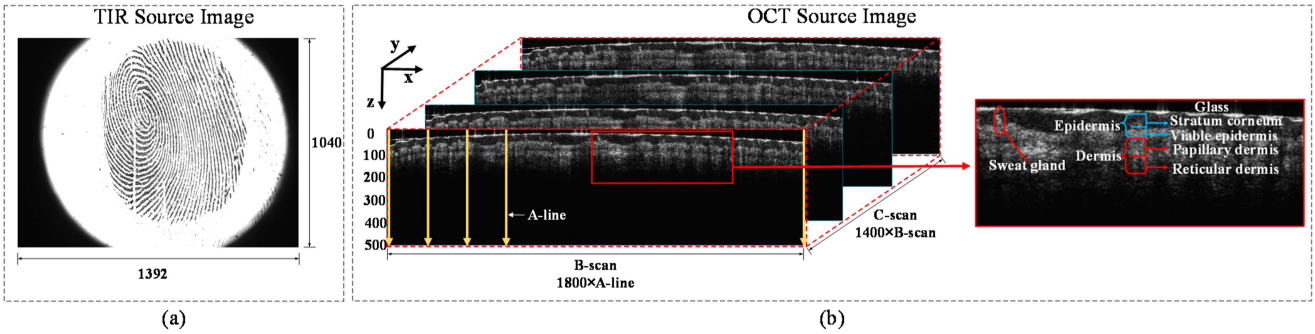

Fig. 3. TIR source image and OCT source images for one finger acquired using the synchronous acquisition system. The image in (a) was collected by TIR acquisition. The images in (b) were collected by OCT acquisition. The skin structure of the finger can be clearly observed in the B-scan images of OCT.

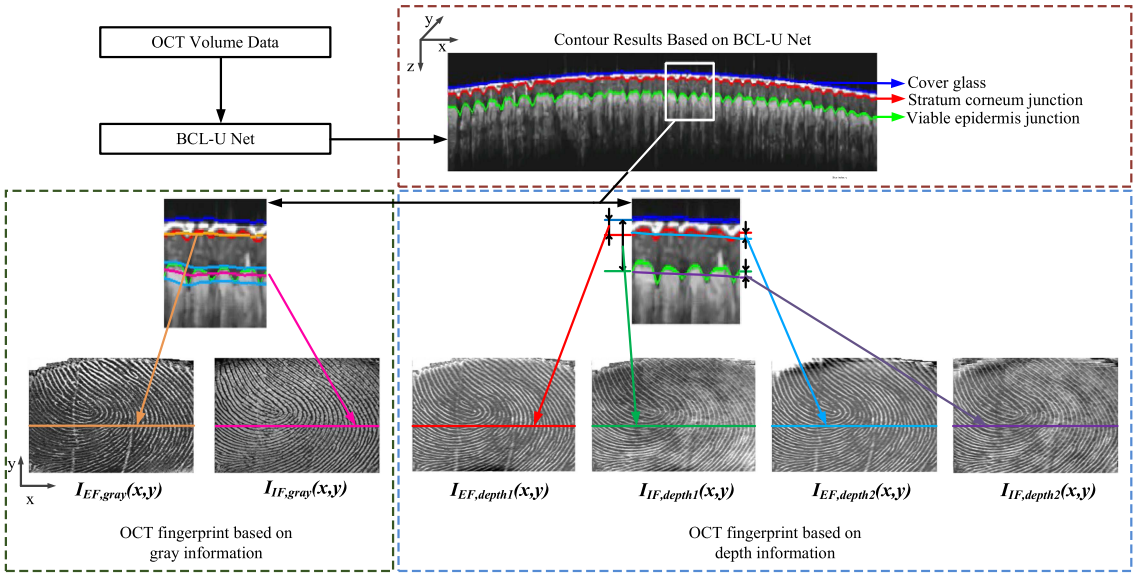

Fig. 4. Overall flow chart from OCT volume data to reconstructed OCT fingerprints in ZJUT-EIFD. Reconstruction method refers to [28], [56].

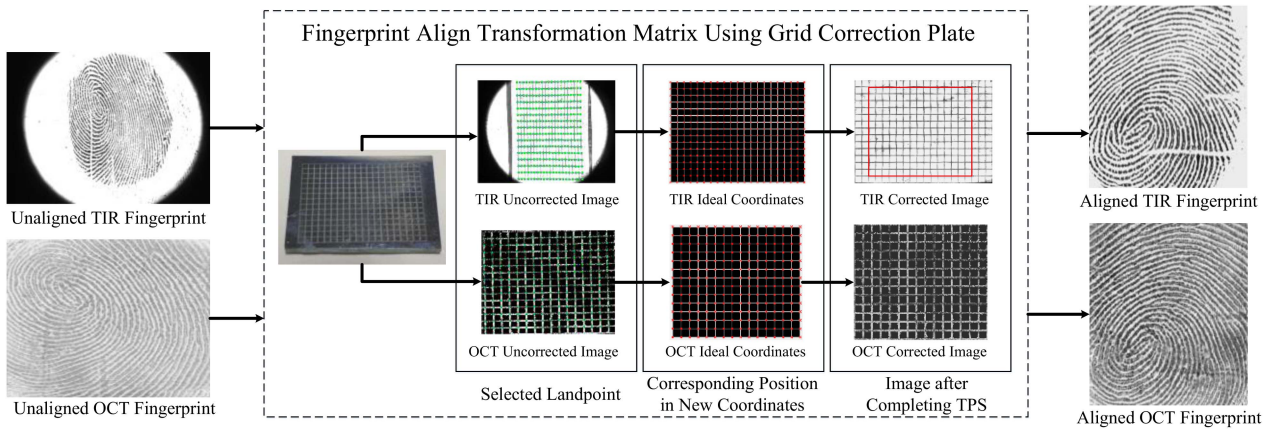

Fig. 5. TIR and OCT fingerprints alignment using grid correction plate [31]. The area of landpoint that can be completely acquired on the OCT image is 15 mm × 13 mm; the TIR corrected image is intercepted to insure the image area consistency. The red rectangle in the TIR corrected image represents the final intercepted area.

TABLE III
COLLECTION DETAILS OF THE DATASET

Subset	Work Classification	Age	Finger*	Number of Volunteer	Number of Finger	Number of Acquisitions	OCT Source Volume Data Size	Collection Interval
dataset-A	White-collar worker	22-30	L1-L4 R1-R4	20	160	1280 (8 times per finger)	1800×1400×500	2 months between two consecutive acquisitions
dataset-B	Blue-collar worker	35-60	L1-L3 R1-R3	10	59**	354 (6 times per finger)	900×700×500	Continuous acquisition
dataset-C	White-collar worker	19-22	L2-L4 R2-R4	30	180	1080 (6 times per finger)	1800×1400×500	Continuous acquisition

*The sequence of numbers (1-4) represents the serial number from Thumb to Ring finger.
**One of the volunteers was missing a finger.

based on this resolution, the fingerprints are all downscaled to 500 dpi for public access and quantitative evaluation.

C. Fingerprint Database Construction

The database is categorized according to the work environment, age, and collection interval of the volunteers. ZJUT-EIFD were divided into three subsets, namely dataset-A, dataset-B, and dataset-C. The differences of each subset are detailed in Table III. In dataset-A, data were first collected for each volunteer four times (orders 1–4). After a two-month interval, data were collected again four times from the same finger (orders 5–8). In dataset-B, in order to ensure that blue-collar workers do not shake their fingers during acquisition, we reduce the resolution of OCT sampling to improve the acquisition speed. In both dataset-B and dataset-C, data were collected six times continuously with position variation. For each identity in each subset, the original source data of TIR image and OCT volume data are kept. Their corresponding TIR and OCT fingerprints at 500 dpi are extracted and stored.

Furthermore, in order to facilitate future researchers to study the relationship between different internal structures of fingers, we label 864 B-scans from our dataset according to the internal hierarchical structure. An example of one of the labels is shown in Fig. 6. These manual labels are made public with ZJUT-EIFD.

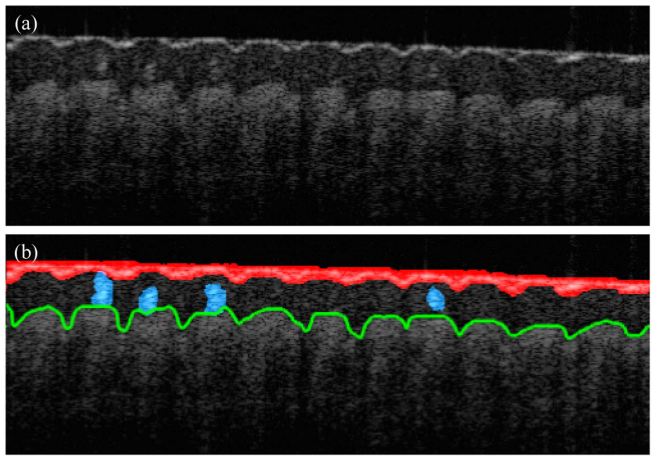

Fig. 6. (a) Example of OCT finger cross-sectional images and (b) its corresponding structure labels. The red area indicates the stratum corneum and glass layers. The blue areas indicate the locations of the subcutaneous sweat glands. The green curve represents the contoured localization of the viable epidermal layer.

IV FINGERPRINT REPRESENTATION

Owing to the difference in imaging methods and fingerprint reconstruction methods, the IF and EF have their own characteristics. In this section, we demonstrate the fingerprints in ZJUT-EIFD and evaluate their qualities.

A. EF and IF Representation

As shown in Fig. 7, we present three sets of fingerprints collected synchronously in ZJUT-EIFD for demonstration. The following can be primarily observed. Firstly, comparing TIR and OCT fingerprints, it can be clearly observed that OCT fingerprints reconstructed by different generation methods all have comparable low contrast. In the case of acceptable hand conditions, the TIR fingerprint is still the first choice for fingerprint recognition compared to the OCT fingerprint.

Secondly, gray_IFs have clearer ridge information compared to the depth-based IFs. Grayscale fingerprints do not depend strongly on the accuracy of contour extraction, but rely more on pixel information. In contrast, depth fingerprint completely relies on the accuracy of contour extraction, localized blurring occurs when contours are lost. Compared with EF, IF by depth is more affected by the contour accuracy. It is mainly due to the extraction area of IF being deeper into the finger tissue. For OCT imaging, deeper depth means a weaker returned signal resulting in poorer imaging quality.

Although the TIR fingerprints get higher contrast, the quality of TIR fingerprints suffers from the unstable condition of the fingertips. Poor skin conditions can lead to a rapid decline in the quality of TIR fingerprints. As shown in Fig. 8, we present some representative fingerprint images in ZJUT-EIFD. These conditions were defined as permanent hand conditions and temporary hand conditions. Wear, tear and irrecoverable scratches are considered permanent hand conditions. Dry and wet are considered temporary hand conditions. When the defects are permanent, the fingerprints collected by OCT can make up for the defects of these TIR fingerprints to a certain extent. As shown in Fig. 8(a), fingerprint wear is common to blue-collar workers,

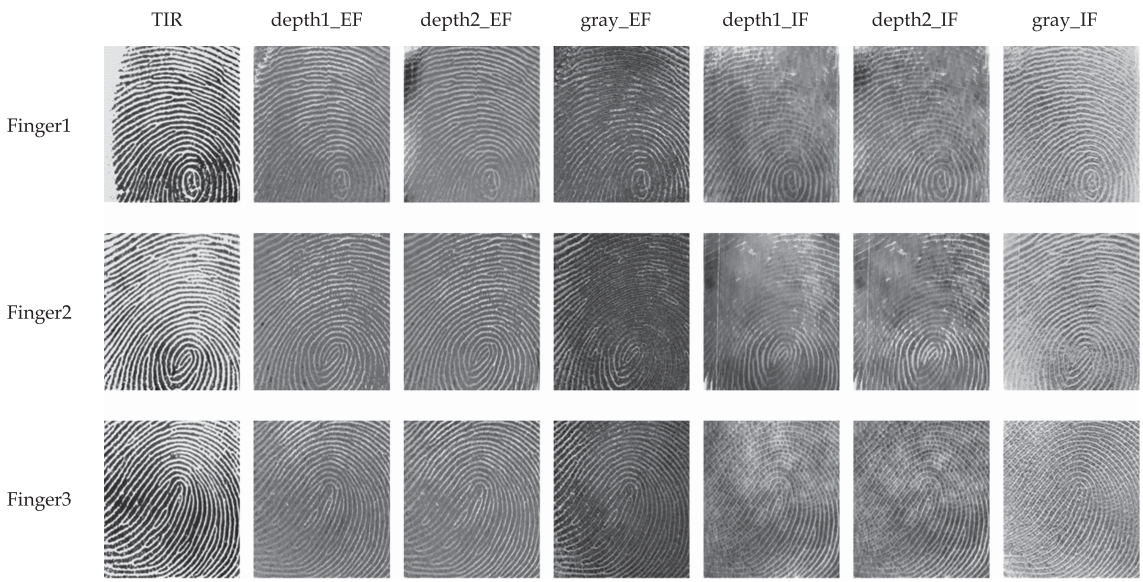

Fig. 7. Fingerprint examples of three fingers. Seven different kinds of fingerprints can be generated by processing the source data after single synchronous acquisition.

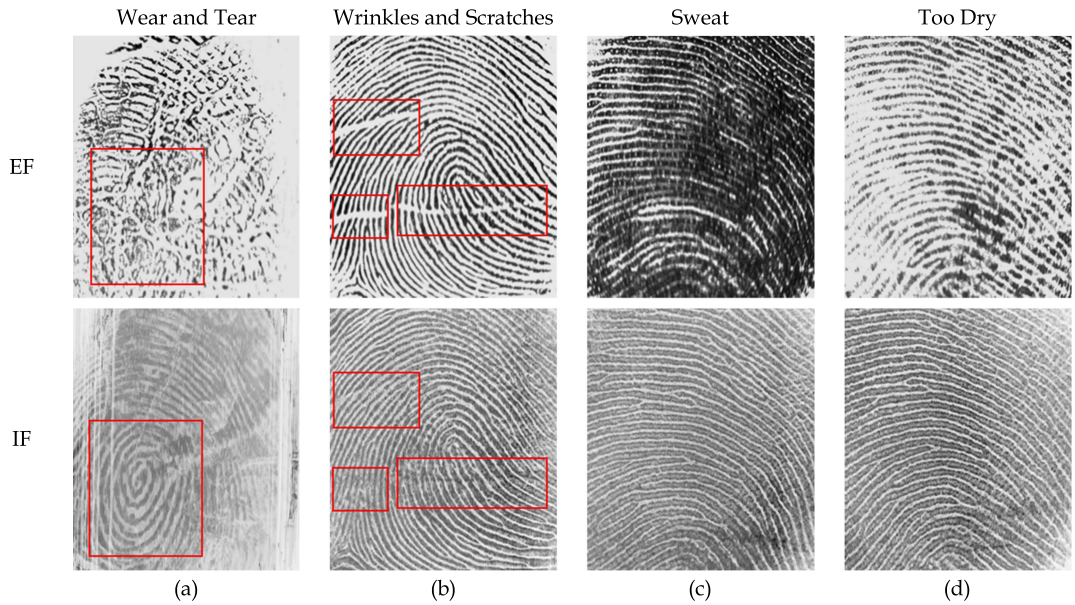

Fig. 8. Some special examples of corresponding EFs and IFs. EF is the TIR fingerprint. IF is the OCT gray_IF obtained by the BCL-U gray method. (a) Wear and tear on fingerprint. (b) Wrinkles and scratches on fingerprint. (c) and (d) Fingerprints captured from the same finger when the finger was wet or dry, respectively. The effects of conditions (a) and (b) are considered permanent, while the effects of conditions (c) and (d) are considered temporary.

especially hand workers. As shown in Fig. 8(b), compared with EF, IF can reduce or even eliminate the negative effects of wrinkles and scratches. When the defects are temporary such as wet and dry conditions, OCT IFs are not affected, as shown in Fig. 8(c) and (d). Thus, IFs can be used as a supplement to EF, thereby improving the recognition ability of distorted fingerprints.

B. *Quality Assessment of EF and IF*

Publicly available NIST finger image quality evaluator (NFIQ2.0) [79] was used here to evaluate our fingerprints. The NFIQ2.0 score ranges from 0 to 100. A higher score means a higher quality fingerprint. The statistical boxplot of NFIQ2.0 scores of EF and IF with different generation methods in our database are shown in Fig. 9. The mean of NFIQ2.0 scores aims to be high, whereas the 1.5IQR (interquartile range) aims to be small.

As shown in Fig. 9, the phenomenon is generally consistent with the above observations. The fingerprints belonging to TIR_EF and gray_IF have the highest overall scores. Depth1_EF, depth2_EF, and gray_EF are slightly lower, Depth1_IF and depth2_IF get the lowest average scores of NFIQ2.0. Horizontally comparing gray_IF and TIR_EF,

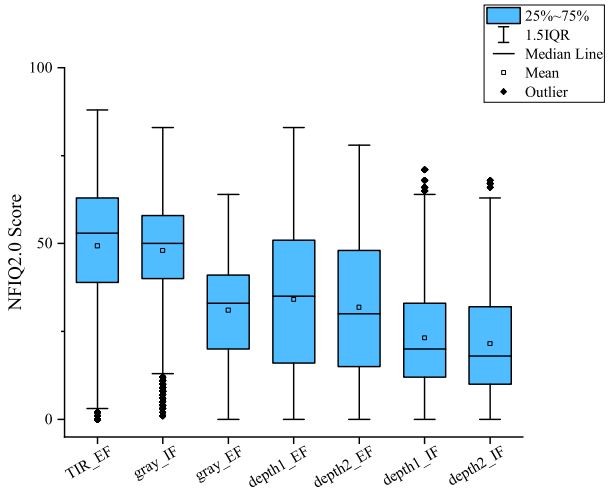

Fig. 9. Boxplot of NFIQ2.0 scores of EF and IF in ZJUT-EIFD.

TIR_EF gets the highest average score but gray_IF has a narrower 1.5IQR. It indicates that fingerprints in TIR_EF have higher fingerprint quality while fingerprints in gray_IF are more stable. There are mainly two factors that result in the distribution of all these scores. The first is the characteristics of OCT imaging. The extracted area of IF is deeper than that of EF, indicating that the returned light signal is weaker, resulting in poor contrast in the IF area in the images of OCT. This poor imaging quality may lead to a local loss of the contours in IF extraction. The second is that depth fingerprints rely more on accurate contour extraction. Once the predicted contour is lost, the pattern of the IF cannot be obtained. Furthermore, we notice that there are also many outliers in the NFIQ2.0 score of gray_IF. This is mainly due to two reasons. On the one hand, permanent hand condi-tions in dataset-B have actually seriously affected the completeness of the internal structure of the fingers. On the other hand, the fingerprint reconstruction algorithm still needs to be improved.

It's worth noted that, the depth-based fingerprint can be affected less by OCT speckle noise since it only cares about the position of the contour rather than the specific gray value in the OCT B-scan image. A more accurate contour extraction algorithm can result in higher contrast patterns in depth-based fingerprints and also improve grayscale-based fingerprints. The depth-based fingerprint also shows more anti-counterfeiting potential. Therefore, we consider that depth-based OCT fingerprints have great potential for development. How to combine the advantages of depth fingerprints and grayscale fingerprints to obtain better quality OCT fingerprints remains to be further studied.

V Verification Performance of ZJUT-EIFD

In this section, we conduct a comprehensive evaluation of the interoperability and verification capabilities of TIR fingerprints and OCT fingerprints in ZJUT-EIFD. The commercial fingerprint matcher VeriFinger 11.1 SDK [80] and a state-of-the-art deep learning-based method DeepPrint [81] were employed for matching experiments to objectively reflect the verification performance. The VeriFinger mainly relies on minutiae points for verification while the DeepPrint estimates features from both image texture and minutiae for verification. It is noteworthy that, to ensure the robust generalization capabilities of DeepPrint, the training data encompassed not only benchmark datasets of FVC2004 and CASIA-Fingerprint but also synthetic fingerprints generated via the utilization of Anguli [82], an open-source implementation of the SfinGe [7]. The final training data includes 341k fingerprints from 44131 unique fingers. The proposed database was not involved in training.

A. Verification Performance of Each Subset

To assess the matching efficacy across distinct fingerprint categories within each subset, we conduct separate matching experiments for different types of fingerprints in each subset. Fingerprints of the same finger were taken as one class, and fingerprints of different fingers were taken as different classes.

For dataset-A, we get 160 classes, thus there are 4480 (160×28) genuine matches and 12720 ($160 \times 159/2$) imposter matches in each types of fingerprints. For dataset-B, we get 59 classes, thus there are 885 (59×15) genuine matches and 1711 ($59 \times 58/2$) imposter matches in each type of fingerprints. For dataset-C, we get 180 classes, thus there are 2700 (180×15) genuine matches and 16110 ($180 \times 179/2$) imposter matches in each type of fingerprints. Note that symmetric matches of the same pair as well as matches between the same images are excluded. The detection error tradeoff (DET) curves of each subset are shown in Fig. 10, where Fig. 10(a)–(c) represent the matching results based on grayscale fingerprints, and Fig. 10(d)–(f) represent the matching results based on depth fingerprints. The DET curve plots the false match rate (FMR) against false non-match rate (FNMR). The FMR is the rate at which a matcher mismatches fingerprints from two distinct individuals as coming from the same individual. The FNMR is the rate at which a matcher miscategorizes two fingerprints from the same individual as being from different individuals. For the same FMR, the lower FNMR indicates the higher matching performance. The equal error rates (EERs) of different subsets are illustrated in Table IV.

Based solely on the outcomes derived from the VeriFinger experiments, we can make the following observations. First of all, it is obvious that the depth-based OCT fingerprints exhibit comparative verification deficiency when compared with grayscale-based OCT fingerprints and TIR fingerprints. Depth-based OCT fingerprints only rely on different depths of the finger structure. As a new type of fingerprint, depth-based fingerprints are quite different from traditional fingerprints in terms of intensity distribution, contrast and so on, which leads to a low fitness to the minutiae-based matching algorithm and thus makes depth-based fingerprints disadvantageous in matching performance. Secondly, gray_IF obtained similar performance with TIR in dataset-A and dataset-B, and surpassed TIR in dataset-C. It shows the potential of the fingerprint collected by OCT in application prospect. Thirdly, the performances of OCT EF are slightly worse than TIR or OCT_IF (both gray and depth),

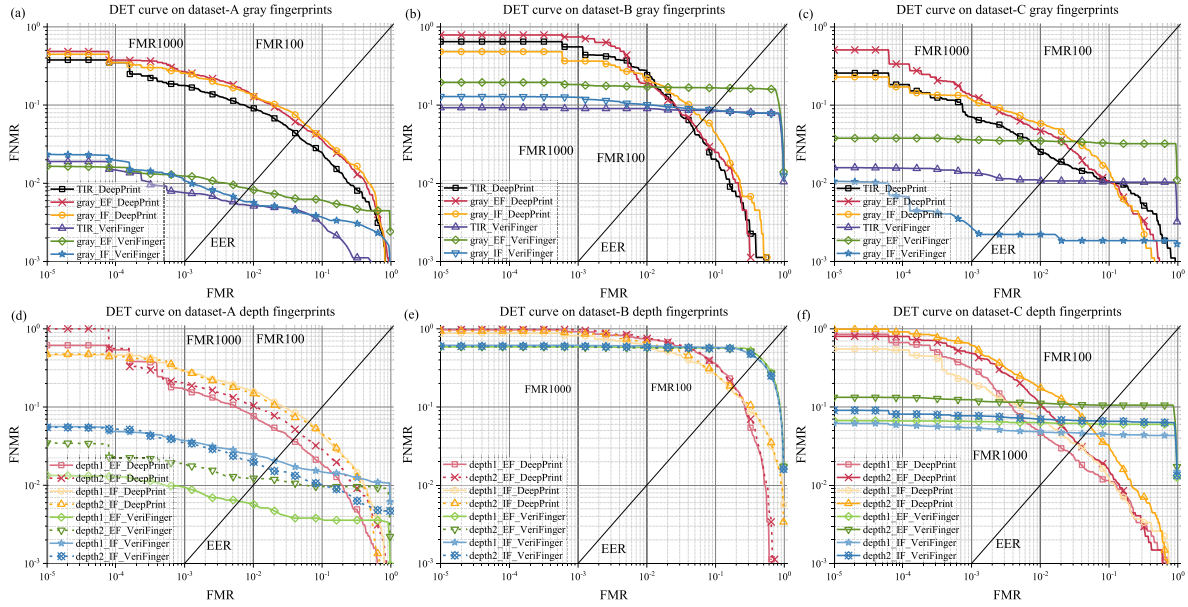

Fig. 10. DET curves of each subset by VeriFinger and DeepPrint. (a)–(c) Represent the verification performances of grayscale-based fingerprints of each subset. (d)–(f) Represent the verification performances of depth-based fingerprints of each subset.

TABLE IV
EERs OF ZJUT-EIFD WITH SEVEN FINGERPRINT TYPES (VERIFINGER/DEEPPRINT)

	TIR	depth1_EF	depth1_IF	depth2_EF	depth2_IF	gray_EF	gray_IF
dataset-A (%)	0.560/4.241	0.623/3.772	2.045/6.431	1.221/4.598	1.636/6.171	0.851/5.312	0.619/5.645
dataset-B (%)	8.474/4.859	43.688/18.531	41.087/16.949	43.371/18.118	41.401/17.417	16.492/5.260	8.740/6.441
dataset-C (%)	1.074/1.889	6.079/2.630	4.550/3.370	10.593/3.481	6.667/5.506	3.425/2.741	0.222/3.389
whole dataset (%)	1.587/3.298	8.452/3.908	8.737/5.392	10.306/5.629	9.073/6.773	3.325/4.345	1.335/4.662

which is probably due to the quality degradation caused by close contact of the finger with the acquisition window.

In contrast to the minutiae-based approach employed by VeriFinger, the learning-based DeepPrint framework amalgamates existing fingerprint minutiae features with fingerprint texture representation, yielding different performances in our experimental assessments. Firstly, as illustrated in Fig. 10(e) and (f), the verification performance of depth-based OCT fingerprints under the DeepPrint is overall better than that achieved by VeriFinger. As presented in Table IV, when deploying DeepPrint for verification experiments, the most pronounced enhancement in performance for depth-based OCT fingerprints is observed within dataset-B (EER reduced by more than 50%). This observation underscores the matching potential for further development of depth-based OCT fingerprints in the field of fingerprint recognition. Secondly, the verification performance of IFs is generally weaker than that of EFs. On the one hand, network training involving only EF will cause data adaptability problems. On the other hand, the texture representation of IF is relatively smooth-varying because it comes from inside the physiological tissue. While the texture representation of EF suffers from uncontrollable hand conditions, which are considered disturbance in conventional matchers but become useful information as distinctive intensity distribution in DeepPrint.

B. *Whole Database Verification Experiment*

Considering that the number of fingerprints in the three subsets is not large, we use all the fingerprints of the same type in the three subsets for matching experiments to verify the recognition performance of the full dataset. Thus we get a total of 399 (160+59+180) classes. Finally, there are 8065 (4480+885+2700) genuine matches and 79401 (399 × 398/2) imposter matches in each type of fingerprint. The DET curves of full database are shown in Fig. 11. The EERs of the full database verification experiment are illustrated in Table IV.

From the results of VeriFinger, it can be clear that the verification performance of TIR and gray_IF is close and better than other types of fingerprints. In fact, EF is prone to permanent changes (scars, abrasions, etc.) in manual workers. Using IF as a complement/replacement of EF to avoid the matching performance degradation caused by permanent changes can be a new direction. It is worth mentioning that the stability and uniqueness of IF still need to be evaluated with a larger database.

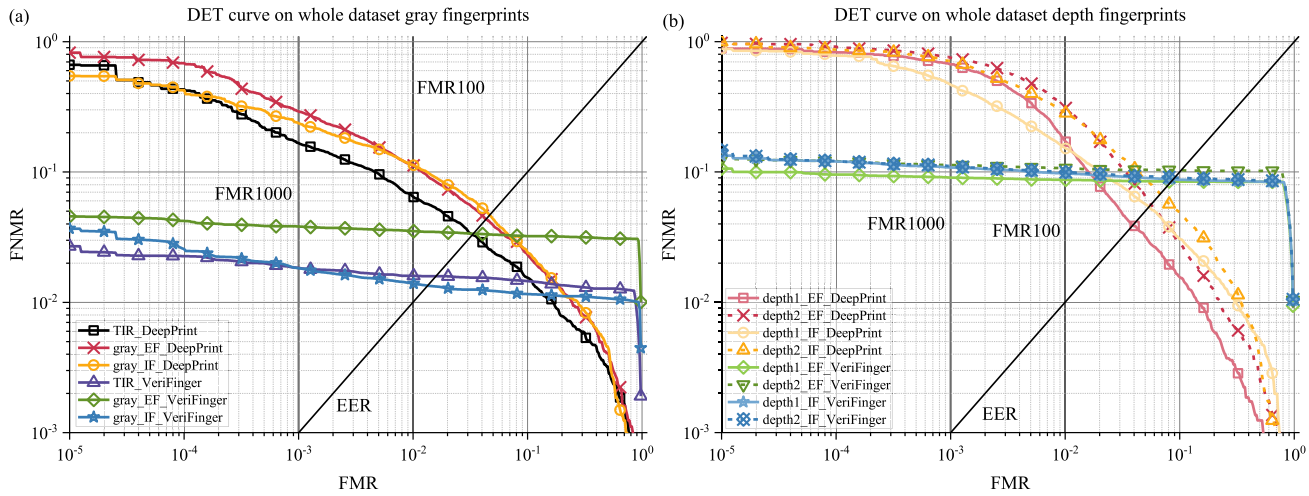

Fig. 11. DET curves of whole database. (a) Represents the verification performance of grayscale-based fingerprints. (b) Represents the verification performance of depth-based fingerprints.

	TIR	depth1_EF	depth2_EF	gray_EF	depth1_IF	depth2_IF	gray_IF
genuine match pair		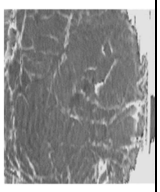	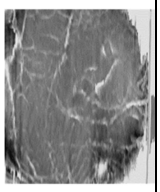	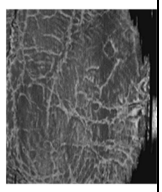		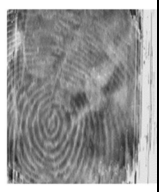	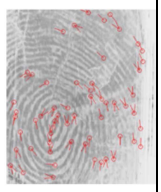
		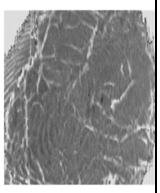	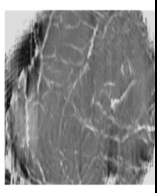	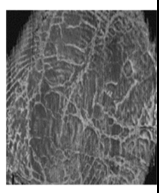	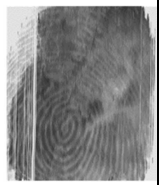	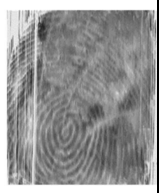	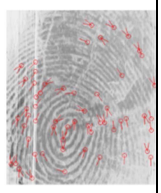
Verifinger Score	0	0	0	0	0	0	139
DeepPrint Score	0.93	0.96	0.97	0.97	0.89	0.84	0.87

Fig. 12. Hard genuine match example when using VeriFinger. The VeriFinger match score of 0 means that the matching pair is completely unrecognizable. Wear-induced degradation adversely affects the extraction of minutiae points, resulting in significantly reduced genuine VeriFinger matching scores. In this group of fingerprints, only gray_IF can use VeriFinger to obtain minutiae. Meanwhile, the maximum match score for DeepPrint is 1. The displayed fingerprint matching pairs here all obtained high DeepPrint scores. The DeepPrint demonstrates the capacity to obtain high genuine matching scores even in the presence of wear-related challenges.

Therefore, expanding data and collection interval will also be our focus in the future.

The results obtained from DeepPrint reveal a close verification performance between depth-based fingerprints and grayscale-based fingerprints compared to VeriFinger. In addition, DeepPrint demonstrates a lower EER when processing depth-based fingerprints in comparison to VeriFinger. This observation underscores the substantial matching potential in depth-based OCT fingerprints.

It is noteworthy that the DET curves generated by VeriFinger are pronounced near-horizontal in Fig. 11, indicating the presence of low genuine matching scores. To illustrate the potential reasons, we present a set of hard genuine match examples for VeriFinger in Fig. 12. As evident in this example, the performance of VeriFinger and DeepPrint is very different. It's obvious that the fingerprint quality degradation caused by wear and aging makes it hard for VeriFinger to obtain minutiae information leading to a notable decline in the genuine matching scores. In this case, only gray_IF can use VeriFinger to obtain minutiae for a good matching score. In contrast, the wear-induced fingerprint degradation introduces distinctive texture representation resulting in high genuine matching scores using DeepPrint. Besides, the genuine matching score of EF is generally higher than that of IF by DeepPrint, which is consistent with DET curve observations in whole datebase (Fig. 11). It is possible to convert permanent fingerprint degradation (wear, wrinkles, aging) into discriminating features. Therefore, in the results of DeepPrint, the performance of EF surpasses IF when

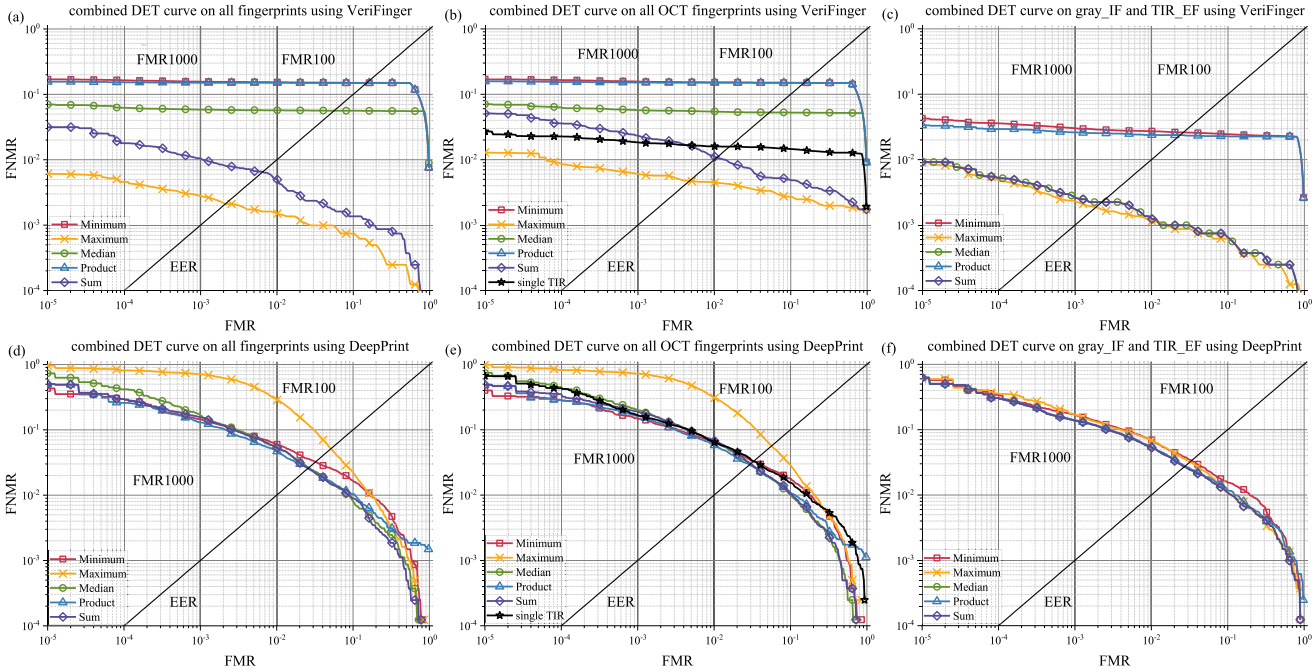

Fig. 13. DET curves of different combination strategies. (a)–(c) Represent the combination performances obtained using VeriFinger. (d)–(f) Represent the combination performances obtained using DeepPrint.

TABLE V
EERs OF DIFFERENT COMBINATION STRATEGIES (VERIFINGER/DEEPPRINT)

Combination strategy	All fingerprints	All OCT fingerprints	gray_IF and TIR_EF
Minimum (%)	15.003/3.226	14.983/3.261	2.605/3.360
Maximum (%)	0.211/5.133	0.473/5.639	0.187/3.224
Median (%)	5.617/2.644	5.270/2.988	0.223/2.703
Product (%)	14.954/2.591	14.941/2.912	2.368/2.740
Sum (%)	6.523/2.549	1.084/3.025	0.223/2.703

no minutiae is presented. Since the collection interval of the proposed dataset is not long, resulting in the texture representation of EFs being relatively close. It is difficult to tell how the texture representation degradation over time will affect the matching effect, where further studies are expected.

C. Verification Experiment With Combined Features

From the full database verification experiment, it can be found that TIR_EF and gray_IF can obtain better performance than other fingerprints when using VeriFinger. Compared with the obvious differences in EER values when using VeriFinger, the performance of various types of fingerprint verification using DeepPrint are relatively close. Notably, pairs of fingerprints that are mismatched by different types of fingerprints would not necessarily overlap. To explore complementary information by different types of fingerprints in ZJUT-EIFD, three combinations of fingerprint are considered, the combination of all fingerprints, the combination of all OCT fingerprints, and the combination of gray_IF and TIR_EF. We use combination strategies in the literature [83] to combine the matching score including the minimum rule, the maximum rule, the median rule, the product rule, and the sum rule. Consistent with the previous section, there are 8065 (4480+885+2700) genuine matches and 79401 (399 $\times$ 398/2) imposter matches. The results are shown in Fig. 13. All of these EER results are shown in Table V.

From the results, we can draw following observation. Firstly, whether it is VeriFinger or DeepPrint, the verification performance can be further improved by appropriate combination rules. For different matcher, the best rule is different. The maximum rule with VeriFinger achieves the best performance in all three fingerprint combinations, and exceeds the matching performance of any single fingerprint. In contrast, except maximum rule, other combination rules with DeepPrint achieve certain performance improvements. Thus, a score combination approach holds considerable promise for enhancing matching performance. The use of specific rules requires comprehensive consideration based on fingerprinting and matching methods. Secondly, the performance improvement is especially significant when using VeriFinger. The best performance occurs in

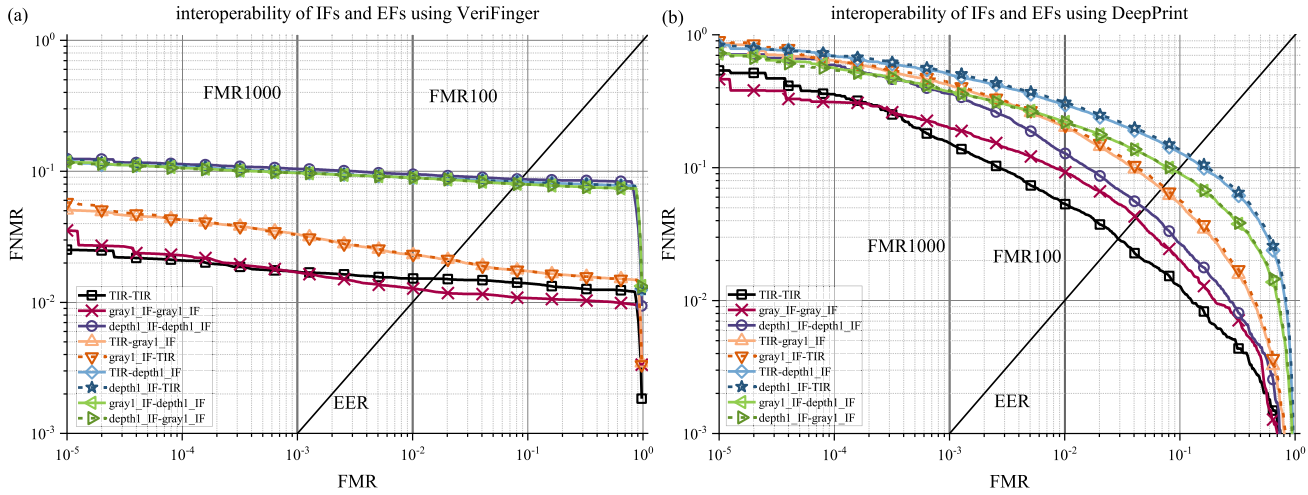

Fig. 14. DET curves of interoperability results. (a) Represents the interoperability results using VeriFinger. (b) Represents the interoperability results using DeepPrint.

combinations of gray_IF and TIR_EF in our database when using VeriFinger. It proves that there is complementary information in the matching of IFs and EFs. Thirdly, as shown in Fig. 13(b) and (e), the best performance of all OCT fingerprints exceeds TIR_EF. The EER of OCT combined performance is reduced by 70.2% ((1.587-0.473)/ 1.587) compared to TIR_EF using VeriFinger. The EER of OCT combined performance is reduced by 11.7% (3.298-2.912)/3.298) compared to TIR using DeepPrint. These performances show the great potential of OCT fingerprints to surpass TIR_EF performance in fingerprint recognition.

D. Interoperability of IFs and EFs

The purpose of the interoperability experiment is to test whether the fingerprint images of different generation methods or from different sensors are compatible with each other. Considering that both TIR and OCT gray_IF achieved good performance in the previous VeriFinger matching experiments, TIR and all types of IF were used for in-teroperability experiments. In this experiment, we evaluate the matching performance using different combinations of TIR_EF, gray_IF and depth1_IF. In each combination, one of them is only the enrollment images, and the other is only the probe images. Each set of experiments contains 158802 ((160+59+180)×(160+59+180-1)) imposter pairs and 18844 ($160 \times 8 \times 8+59 \times 6 \times 6+180 \times 6 \times 6$) genuine pairs. The results for these matching experiments are shown in Fig. 14 and Table VI. In the legend, enrollment images are on the left, and probe images are on the right.

From the matching results, we have three observations. Firstly, whether VeriFinger or DeepPrint is configured for matching, the best performance is obtained in TIR-TIR and gray_IF-gray_IF. It indicates that the gray_IF acquired by OCT has a strong verification potential. Secondly, whether using VeriFinger or DeepPrint, the recognition performance of mix gray_IF and TIR_EF set (TIR images are used to enroll, gray_IF images are used to probe, and vice versa) only drops slightly compared to single dataset. Especially when using VeriFinger, interoperability matching performance is quite high under stringent operating points (FMR1000<4%, EER<3%). This indicates that the IF acquired by OCT is compatible with the traditional fingerprint by TIR. Thirdly, it is notable that, with the exception of depth1_IF, VeriFinger consistently yields lower EER values compared to DeepPrint across various combinations. The reason is that when the enrollment and probe fingerprints belong to different categories, it is difficult to extract valuable texture information for matching. Under such circumstances, the utilization of traditional minutiae-based fingerprint algorithms remains a pragmatic and effective choice.

TABLE VI
EERs OF INTEROPERABILITY OF IFs AND EFs (VERIFINGER/DEEPPRINT)

enrollment	probe	EER
TIR_EF	TIR_EF	1.517/2.908
gray_IF	gray_IF	1.245/4.181
depth1_IF	depth1_IF	8.693/4.929
TIR_EF	gray_IF	2.119/6.905
gray_IF	TIR_EF	2.122/7.228
TIR_EF	depth1_IF	8.327/11.892
depth1_IF	TIR_EF	8.311/12.343
gray_IF	depth1_IF	8.029/9.345
depth1_IF	gray_IF	8.005/9.382

E. Synchronization Performance Comparison

Synchronous acquisition can reduce the distortion and deformation of fingerprints, making the research on the correlation between internal and external fingerprints more convenient. To verify the effectiveness of synchronous acquisition, we counted the genuine matching scores of 1742 ($160 \times 8+59 \times 6+18 \times 6$) sets synchronous acquisition and the genuine matching scores of

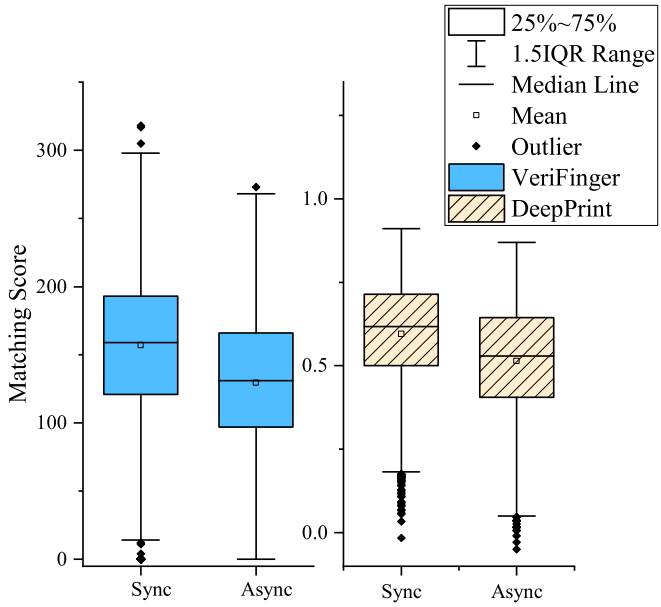

Fig. 15. Boxplot of corresponding synchronous and asynchronous genuine matching scores between TIR_EF and gray_IF.

TABLE VII
STATISTIC OF SYNCHRONOUS AND ASYNCHRONOUS GENUINE MATCHES (VERIFINGER/DEEPPRINT)

Statistic	Sync	Async
Mean	157/0.596	129/0.515
Median(Q2)	159/0.618	131/0.529
Q1	121/0.500	97/0.406
Q3	193/0.714	166/0.644
Max	318/0.911	273/0.870
Min	0/-0.016	0/-0.050

1742 ($160 \times 8+59 \times 6+18 \times 6$) sets asynchronous acquisition. Only TIR_EF and gray_IF are used for this evaluation. Synchronous and asynchronous performance experiences perform only one genuine match of each fingerprint classes, respectively.

The statistics boxplot of corresponding synchronous and asynchronous genuine matching scores are shown in Fig. 15. The corresponding statistics values are shown in Table VII. The overall scores of genuine matches with synchronous acquisitions are higher. Compared with asynchronous acquisition, the mean genuine matching score of synchronous acquisition by VeriFinger and DeepPrint is increased by 21.7% (157/129-1) and 15.7% (0.596/0.515-1), respectively. Other statistical values, including maximum, median (Q2), lower quantile (Q1) and upper quantile (Q3), were all improved. It intuitively reflects the effectiveness of synchronous acquisition. Note that the minimum genuine matching scores of the statistics are all near 0 by using VeriFinger and DeepPrint. The very poor quality of certain fingerprints (either EF or IF) will result in not being able to find enough minutiae information, leading to matching scores of 0 using VeriFinger. DeepPrint calculates the matching score based on cosine similarity. The lack of minutiae and large differences

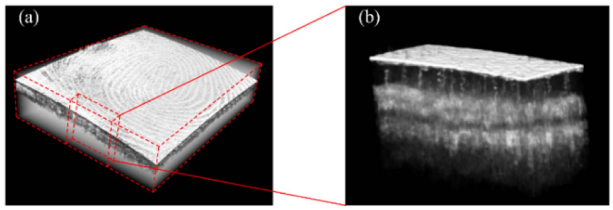

Fig. 16. OCT 3D volume data. Rendering via inviwo. (a) OCT source data. (b) Sweat glands are clearly visible in OCT source data.

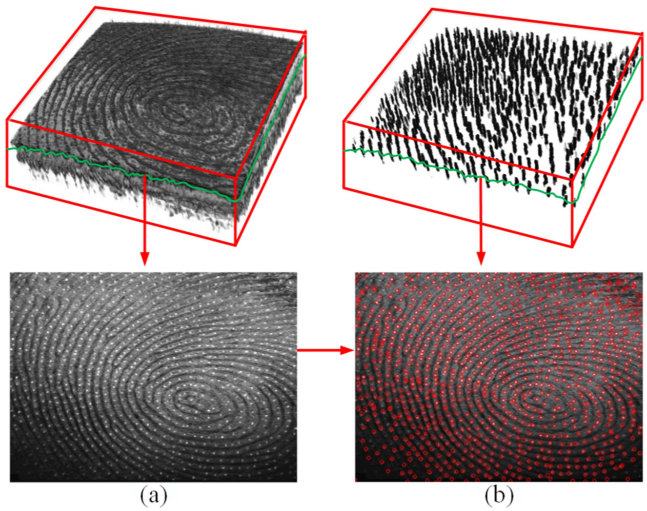

Fig. 17. Example of sweat pore reconstruction in [28], (a) the image generated by the intensities at lines between the contours of stratum corneum and the viable epidermis junction, (b) the predicting results with red circles indicating the sweat pores' locations.

in texture will cause the scores to be close to 0. In fact, no fingerprint quality-related enrollment restriction is performed in the proposed database. On the contrary, some highly distorted fingerprints are purposely acquired for distortion related researches. In the real life scenarios, a fingerprint quality selection method usually adopted to reject very poor quality samples.

VI DISCUSSION

To demonstrate the application potential of ZJUT-EIFD, we discuss some promising directions.

A. 3D OCT Volume Data Recognition

What OCT essentially acquires is the physiological structure information inside the finger. As shown in Fig. 16(a), the subcutaneous structure of the finger contains recognication information such as unique fingerprint patterns and sweat gland locations. Skin differences between different individuals can also be intuitively observed through the 3D OCT volume data. Directly using 3D volume data for matching is promising.

B. Fused Fingerprint Recognition

The purpose of fingerprint fusion is to generate reliable fingerprint representation with better recognition performance.

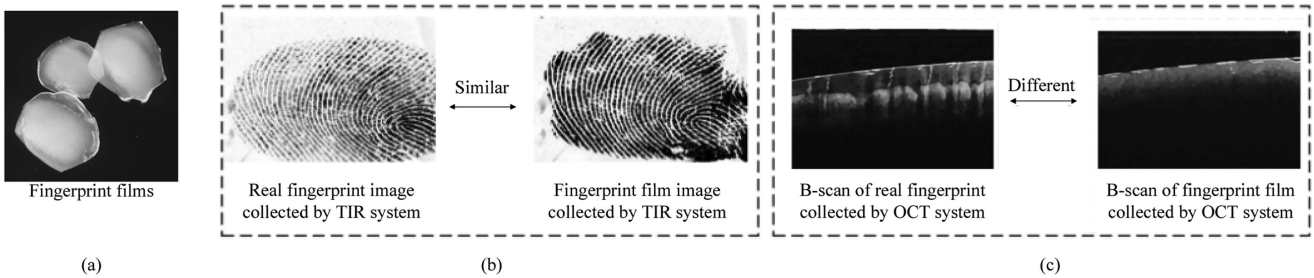

Fig. 18. Anti-spoofing example [91]. (a) Fingerprint films; (b) fingerprints of real finger and fake fingerprint film collected by traditional TIR system; (c) B-scans of real finger and fake fingerprint film collected by OCT system.

Depending on the data used, there can be different types of fingerprint fusion.

For OCT data only, according to the fingerprint reconstruction results of different depth structures, the stratum corneum, active epidermal fingerprints, etc. can be generated. Therefore, information from various subsurface fingerprints can be fused to form a robust fingerprint representation with stronger recognition performance. Some research results can be found in [49].

Benefiting from the simultaneous acquisition of TIR and OCT, it is possible for us to fuse these two different types of fingerprints. Valid information from TIR and OCT can be fused to generate new fingerprint representations that not only have the high contrast and usually good image quality of TIR, but are resistant to non-ideal hand conditions such as wrinkles, wetness, aging, etc.

C. High Resolution Fingerprint Recognition

The fingerprint resolutions published in ZJUT-EIFD are all 500 dpi. In fact, the resolution of OCT (dataset-A and dataset-C: 2540 dpi, dataset-B: 1270 dpi) and TIR (lateral 820 dpi, vertical 1650 dpi) source data is higher than 500 dpi. Based on the source data, higher resolution fingerprint images can be obtained. We note that high-resolution fingerprints can further improve the recognition performance by utilizing the extended feature set (especially sweat pores) [8], [84], [85]. However, there are still less recognition attempts on high-resolution OCT fingerprints. Using ZJUT-EIFD to generate high-resolution EF and IF and study their recognition capabilities has a promising future.

D. Subcutaneous Sweat Glands Recognition

As shown in Fig. 16(b), the subcutaneous sweat gland is a small gland that secretes sweat. In the inter-OCT volume data, it is located between the stratum corneum and the viable epidermis. The outlets of sweat glands in the epidermis are sweat pores. Sweat pores as one of the level-3 features of fingerprints are also claimed to be permanent, immutable and unique according to forensic experts [86], [87], so as the sweat glands. If properly utilized, sweat glands can provide authenticating information for human identification. As shown in Fig. 17, it is possible to obtain subcutaneous sweat glands using OCT and find corresponding sweat pores based on their location. Furthermore, direct recognition using the morphology and distribution of sweat glands is also promising, whose prerequisite is precise segmentation of the sweat gland position. Some research results can be found in [28], [88], [89], [90].

E. Anti-Spoofing

Fingerprint anti-spoofing technology based on OCT has been widely developed. Compared with the anti-spoofing technology based on 2D fingerprints, the 3D representation provided by OCT has greater advantages. As shown in Fig. 18, it is widely considered that replicating the internal structure of a finger is a difficult task. Mainstream OCT anti-spoofing techniques can be roughly divided into methods based on internal depth information [25], [92], [93] and methods based on neural networks [26], [94], [95], [96]. However, due to the difference in internal structure of distinct fingers and the diversity of spoofing samples, it is still a challenging task to establish a general model to achieve high-precision anti-spoofing.

F. Acquisition and Processing Time

Fingerprint recognition technology enjoys widespread popularity within the realm of biometrics, primarily not only owing to its uniqueness and permanence, but also coupled with its capacity for rapid data acquisition and identification. Nevertheless, the practical application of OCT encounters significant challenges due to the considerable time investment entailed in the raw spectrum acquisition and processing, and IF reconstruction. This time constraint presents a hindrance to deploying OCT in time-sensitive environments. Encouragingly, recent research endeavors have yielded promising advancements in addressing these challenges. Through improvements in photosensitive element technology and light source frequency, raw spectrum acquisition speeds of MHz have been achieved [97]. Meanwhile, the adoption of parallel computing GPU acceleration techniques has enabled real-time raw spectrum processing within OCT [98], [99]. Furthermore, lightweight neural networks have estimated IF with quality comparable to that of complex networks, demonstrating the feasibility of rapid IF reconstruction [100]. Consequently, at a resolution of 500 dpi, it is feasible to use OCT to capture fingerprints at a speed comparable to TIR.

It needs to be emphasized that the principal advantage of OCT resides in its capacity to attain ultra-high resolution IF. Therefore, in scenarios where time is not sensitive and fingerprint clarity is required, a mode higher than 500 dpi should still be used for IF acquisition. These scenarios include but not

limited to forensic evidence collection, public security identity record maintenance, and supplementary recording of identity information for people with worn fingerprints.

VII Conclusion

In this article, we present a novel and comprehensive fingerprint database, denoted as ZJUT-EIFD. It provides the rich dataset composition of OCT and TIR data by synchronous acquisition to serve data benchmarking and interoperability testing for EF-IF research. The synchronous acquisition of EF and IF can minimize distortions that may arise and offers distinct advantage on researching the correlation between them. The proposed database includes source data of raw TIR fingerprint images and OCT volume data (partial with labeled B-scan physiological structures), as well as corresponding TIR and OCT fingerprint images at 500 dpi. The construction of the ZJUT-EIFD is described in detail. The quality of fingerprints in ZJUT-EIFD is explicitly demonstrated, which shows the recognition potential of fingerprints in ZJUT-EIFD. Matching experiments were carried out and the recognition characteristics of different fingerprints in ZJUT-EIFD were discussed, which mainly demonstrates the following two points: 1) the recognition performance of the IF acquired by OCT can be close to or even exceed that of traditional EF images (TIR) in specific situations; 2) the IF is compatible with EF.

Despite preliminary matching experiments carried out on EFs and IFs, promising work can be further explored using ZJUT-EIFD, such as the optimization of IF reconstruction methods and the improvement of matching algorithms. Some potential applications of ZJUT-EIFD were discussed in this article, which may provide guidance for future researches. The expansion and improvement of ZJUT-EIFD will become the direction of our future development.

References

[1] S. Prabhakar, S. Pankanti, and A. K. Jain, "Biometric recognition: Security and privacy concerns," *IEEE Secur. Privacy*, vol. 1, no. 2, pp. 33–42, Mar./Apr. 2003.

[2] A. K. Jain, P. Flynn, and A. A. Ross, *Handbook of Biometrics*. Berlin, Germany: Springer, 2007.

[3] A. K. Jain, A. Ross, and S. Prabhakar, "An introduction to biometric recognition," *IEEE Trans. Circuits Syst. Video*, vol. 14, no. 1, pp. 4–20, Jan. 2004.

[4] Q. Xiao, "Technology review - biometrics-technology, application, challenge, and computational intelligence solutions," *IEEE Comput. Intell. Mag.*, vol. 2, no. 2, pp. 5–25, May 2007.

[5] Q. Tao and R. Veldhuis, "Biometric authentication system on mobile personal devices," *IEEE Trans. Instrum. Meas.*, vol. 59, no. 4, pp. 763–773, Apr. 2010.

[6] S. Pankanti, S. Prabhakar, and A. Jain, "On the individuality of fingerprints," *IEEE Trans. Pattern Anal. Mach. Intell.*, vol. 24, no. 8, pp. 1010–1025, Aug. 2002.

[7] D. Maltoni, D. Maio, A. K. Jain, and S. Prabhakar, *Handbook of Fingerprint Recognition*, 2nd ed. Berlin, Germany: Springer, 2009.

[8] A. K. Jain, Y. Chen, and M. Demirkus, "Pores and ridges: High-resolution fingerprint matching using level 3 features," *IEEE Trans. Pattern. Anal. Mach. Intell.*, vol. 29, no. 1, pp. 15–27, Jan. 2007.

[9] C. H. Lin et al., "Fingerprint comparison. I: Similarity of fingerprints," *J. Forensic Sci.*, vol. 27, no. 2, pp. 290–304, Apr. 1982.

[10] A. K. Jain, S. Prabhakar, and S. Pankanti, "On the similarity of identical twin fingerprints," *Pattern Recognit.*, vol. 35, no. 11, pp. 2653–2663, Nov. 2002.

[11] R. Richter, C. Gottschlich, L. Mentch, D. H. Thai, and S. F. Huckemann, "Smudge noise for quality estimation of fingerprints and its validation," *IEEE Trans. Inf. Forensic Secur.*, vol. 14, no. 8, pp. 1963–1974, Aug. 2019.

[12] J. Harvey, J. Campbell, and A. Adler, "Characterization of biometric template aging in a multiyear, multivendor longitudinal fingerprint matching study," *IEEE Trans. Instrum. Meas.*, vol. 68, no. 4, pp. 1071–1079, Aug. 2019.

[13] A. W. Senior and R. M. Bolle, "Improved fingerprint matching by distortion removal," *Inst. Electron., Inf. Commun. Engineers Trans. Inf. Syst.*, vol. 84, no. 7, pp. 825–832, Jul. 2001.

[14] E. Marasco and A. Ross, "A survey on antispoofing schemes for fingerprint recognition," *Assoc. Comput. Machinery Comput. Surv.*, vol. 47, no. 2, pp. 1–36, Jan. 2015.

[15] J. J. Engelsma, S. S. Arora, A. K. Jain, and N. G. Paulter, "Universal 3D wearable fingerprint targets: Advancing fingerprint reader evaluations," *IEEE Trans. Inf. Forensic Secur.*, vol. 13, no. 6, pp. 1564–1578, Jun. 2018.

[16] X. Xia and L. O'Gorman, "Innovations in fingerprint capture devices," *Pattern Recognit.*, vol. 36, no. 2, pp. 361–369, Feb. 2003.

[17] D. Huang et al., "Optical coherence tomography," *Science*, vol. 254, no. 5035, pp. 1178–1181, Nov. 1991.

[18] W. Drexler and J. G. Fujimoto, *Optical Coherence Tomography: Technology and Applications*, 2nd ed. Berlin, Germany: Springer, 2008.

[19] Y. Cheng and K. V. Larin, "Artificial fingerprint recognition by using optical coherence tomography with autocorrelation analysis," *Appl. Opt.*, vol. 45, no. 36, pp. 9238–9245, Dec. 2006.

[20] M. C. Potcoava and M. K. Kim, "Fingerprint biometry applications of digital holography and low-coherence interferography," *Appl. Opt.*, vol. 48, no. 34, pp. 9–15, Dec. 2009.

[21] J. Aum, J.-H. Kim, and J. Jeong, "Live acquisition of internal fingerprint with automated detection of subsurface layers using OCT," *IEEE Photon. Tech. Lett.*, vol. 28, no. 2, pp. 163–166, Jan. 2016.

[22] F. Liu, W. Zeng, W. Zhang, L. Wang, J. Cheng, and Z. Lai, "Multilayered minutiae extraction based on fusion-attention for OCT fingerprints," *IEEE Trans. Biometrics, Behavior, Identity Sci.*, vol. 5, no. 2, pp. 221–232, Apr. 2023.

[23] A. Bossen, R. Lehmann, and C. Meier, "Internal fingerprint identification with optical coherence tomography," *IEEE Photon. Tech. Lett.*, vol. 22, no. 7, pp. 507–509, Apr. 2010.

[24] X. Yu et al., "Contrast enhanced subsurface fingerprint detection using high-speed optical coherence tomography," *IEEE Photon. Tech. Lett.*, vol. 29, no. 1, pp. 70–73, Jan. 2017.

[25] F. Liu, G. Liu, and X. Wang, "High-accurate and robust fingerprint antispoofing system using optical coherence tomography," *Expert Syst. Appl.*, vol. 130, pp. 31–44, Apr. 2019.

[26] F. Liu, H. Liu, W. Zhang, G. Liu, and L. Shen, "One-class fingerprint presentation attack detection using auto-encoder network," *IEEE Trans. Image Process.*, vol. 30, pp. 2394–2407, 2021.

[27] Y. Yu, H. Wang, P. Chen, Y. Zhang, Z. Guo, and R. Liang, "A new approach to external and internal fingerprint registration with multisensor difference minimization," *IEEE Trans. Biometrics, Behavior, Identity Sci.*, vol. 2, no. 4, pp. 363–376, Oct. 2020.

[28] B. Ding et al., "Surface and internal fingerprint reconstruction from optical coherence tomography through convolutional neural network," *IEEE Trans. Inf. Forensics Secur.*, vol. 16, pp. 685–700, 2021.

[29] S. K. Modi, S. J. Elliott, and H. Kim, "Statistical analysis of fingerprint sensor interoperability performance," in *Proc. IEEE 3rd Int. Conf. Biometrics Theory Appl. Syst.*, 2009, pp. 1–6.

[30] S. Moore, "Latest tests of biometrics systems shows wide range of abilities," *IEEE Spectr. Online*, 2004. [Online]. Available: http://spectrum.ieee.org/computing/embedded-systems/latest-tests-of-biometrics-systems-shows-wide-range-of-abilities

[31] H. Sun et al., "Synchronous fingerprint acquisition system based on total internal reflection and optical coherence tomography," *IEEE Trans. Instrum. Meas.*, vol. 69, no. 10, pp. 8452–8465, Oct. 2020.

[32] M. Tartagni and R. Guerrieri, "A fingerprint sensor based on the feedback capacitive sensing scheme," *IEEE J. Solid-State Circuits*, vol. 33, no. 1, pp. 133–142, Jan. 1998.

[33] R. D. Bahuguna and T. Corbolin, "Prism fingerprint sensor that uses a holographic optical element: Response to comment," *Appl. Opt.*, vol. 36, no. 26, pp. 6611–6611, Sep. 1997.

[34] G. Parziale, E. Diaz-Santana, and R. Hauke, "The Surround imager TM: A Multi-camera touchless device to acquire 3D rolled-equivalent fingerprints," in *Proc. Adv. Biometrics: Int. Conf.*, 2005 pp. 244–250.

[35] F. Liu, D. Zhang, C. Song, and G. Lu, "Touchless multiview fingerprint acquisition and mosaicking," *IEEE Trans. Instrum. Meas.*, vol. 62, no. 9, pp. 2492–2502, Sep. 2013.
[36] A. Kumar and C. Kwong, "Towards contactless, low-cost and accurate 3D fingerprint identification," *IEEE Trans. Inf. Forensics Secur.*, vol. 37, no. 3, pp. 681–696, Mar. 2015.
[37] Y. Lu et al., "Ultrasonic fingerprint sensor using a piezoelectric micromachined ultrasonic transducer array integrated with complementary metal oxide semiconductor electronics," *Appl. Phys. Lett.*, vol. 106, no. 26, Jun. 2015, Art. no. 263503.
[38] Y. Wang, L. G. Hassebrook, and D. L. Lau, "Data acquisition and processing of 3-D fingerprints," *IEEE Trans. Inf. Forensics Secur.*, vol. 5, no. 4, pp. 750–760, Dec. 2010.
[39] J. J. Engelsma, K. Cao, and A. K. Jain, "RaspiReader: Open source fingerprint reader," *IEEE Trans. Pattern Anal. Mach. Intell.*, vol. 41, no. 10, pp. 2511–2524, Oct. 2019.
[40] S. A. Grosz, J. J. Engelsma, E. Liu, and A. K. Jain, "C2CL: Contact to contactless fingerprint matching," *IEEE Trans. Inf. Forensics Secur.*, vol. 17, pp. 196–210, 2022.
[41] A. Rattani, W. J. Scheirer, and A. Ross, "Open set fingerprint spoof detection across novel fabrication materials," *IEEE Trans. Inf. Forensics Secur.*, vol. 10, no. 11, pp. 2447–2460, Nov. 2015.
[42] A. Alex et al., "Multispectral in vivo three-dimensional optical coherence tomography of human skin," *Proc. SPIE*, vol. 15, no. 2, Mar. 2010, Art. no. 026025.
[43] E. Auksorius and A. C. Boccara, "Fingerprint imaging from the inside of a finger with full-field optical coherence tomography," *Biomed. Opt. Exp.*, vol. 6, no. 11, pp. 4465–4471, Nov. 2015.
[44] Y. Cheng and K. V. Larin, "In vivo two- and three-dimensional imaging of artificial and real fingerprints with optical coherence tomography," *IEEE Photon. Tech. Lett.*, vol. 19, no. 20, pp. 1634–1636, Oct. 2007.
[45] Y.-P. Liu, Q. Zhong, R. Liang, Z. Li, H. Wang, and P. Chen, "Layer segmentation of OCT fingerprints with an adaptive Gaussian prior guided transformer," *IEEE Trans. Instrum. Meas.*, vol. 71, 2022, Art. no. 5023515.
[46] K. B. Raja et al., "Robust verification with subsurface fingerprint recognition using full field optical coherence tomography," in *Proc. IEEE Conf. Comput. Vis. Pattern Recognit. Workshops*, 2017, pp. 646–654.
[47] M. Liu and T. Buma, "Biometric mapping of fingertip eccrine glands with optical coherence tomography," *IEEE Photon. Technol. Lett.*, vol. 22, no. 22, pp. 1677–1679, Nov. 2010.
[48] A. Zam et al., "Feasibility of correlation mapping optical coherence tomography (cmOCT) for anti-spoof sub-surface fingerprinting," *J. Biophoton.*, vol. 6, no. 9, pp. 663–667, Sep. 2013.
[49] F. Liu et al., "Robust and high-security fingerprint recognition system using optical coherence tomography," *Neurocomputing*, vol. 402, pp. 14–28, Aug. 2020.
[50] J. Sekulska-Nalewajko, J. Gocławski, and D. Sankowski, "The detection of internal fingerprint image using optical coherence tomography," *Image Process. Commun.*, vol. 22, no. 4, pp. 59–72, Dec. 2017.
[51] P. Korohoda, A. Dąbrowski, and P. Pawłowski, "Optical coherence tomography for fingerprint acquisition from internal layer—A case study," in *Proc. Signal Process. Algorithms, Archit., Arrangements, Appl.*, 2014, pp. 176–180.
[52] L. N. Darlow and J. Connan, "Efficient internal and surface fingerprint extraction and blending using optical coherence tomography," *Appl. Opt.*, vol. 54, no. 31, pp. 9258–9268, Nov. 2015.
[53] R. Khutlang and F. V. Nelwamondo, "Novelty detection-based internal fingerprint segmentation in optical coherence tomography images," in *Proc. 2nd Int. Symp. Comput. Netw.*, 2014, pp. 556–559.
[54] L. N. Darlow and J. Connan, "Study on internal to surface fingerprint correlation using optical coherence tomography and internal fingerprint extraction," *Proc. SPIE*, vol. 24, no. 6, Dec. 2015, Art. no. 063014.
[55] H. Wang, L. Ma, and P. Chen, "External and internal fingerprint extraction based on optical coherence tomography," *Proc. SPIE*, vol. 10827, 2018, Art. no. 108271E.
[56] H. Wang et al., "Acquisition and extraction of surface and internal fingerprints from optical coherence tomography through 3D fully convolutional network," *Optik*, vol. 205, pp. 164–176, Mar. 2020.
[57] D. Maio, D. Maltoni, R. Cappelli, J. L. Wayman, and A. K. Jain, "FVC2000: Fingerprint verification competition," *IEEE Trans. Pattern Anal. Mach. Intell.*, vol. 24, no. 3, pp. 402–412, Mar. 2002.
[58] D. Maio et al., "FVC2002: Second fingerprint verification competition," in *Proc. Int. Conf. Pattern Recognit.*, 2002, pp. 811–814.
[59] D. Maio et al., "FVC2004: Third fingerprint verification competition," in *Proc. Int. Conf. Biometric Authentication*, 2004, pp. 1–7.
[60] R. Cappelli et al., "Fingerprint verification competition 2006," *Biometric Technol. Today*, vol. 15, no. 7, pp. 7–9, Aug. 2007.
[61] "NIST biometric special databases and software." May 2010. Accessed: Jul. 2022. [Online]. Available: https://www.nist.gov/itl/iad/image-group/resources/biometric-special-databases-and-software
[62] "NIST special database 4." Aug. 2010. Accessed: Jul. 2022. [Online]. Available: https://www.nist.gov/srd/nist-special-database-4
[63] "NIST special database 14." Aug. 2010. Accessed: Jul. 2022. [Online]. Available: https://www.nist.gov/srd/nist-special-database-14
[64] "CASIA fingerprint image database." Nov. 2016. Accessed: Jul. 2022. [Online]. Available: http://biometrics.idealtest.org/findTotalDbByMode.do?mode=Fingerprint#/datasetDetail/7
[65] X. Si, J. Feng, J. Zhou, and Y. Luo, "Detection and rectification of distorted fingerprints," *IEEE Trans. Pattern Anal. Mach. Intell.*, vol. 37, no. 3, pp. 555–568, Mar. 2015.
[66] J. Feng, Y. Shi, and J. Zhou, "Robust and efficient algorithms for separating latent overlapped fingerprints," *IEEE Trans. Inf. Forensics Secur.*, vol. 7, no. 5, pp. 1498–1510, Oct. 2012.
[67] F. Chen, J. Feng, A. K. Jain, J. Zhou, and J. Zhang, "Separating overlapped fingerprints," *IEEE Trans. Inf. Forensics Secur.*, vol. 6, no. 2, pp. 346–359, Jun. 2011.
[68] C. Lin and A. Kumar, "Tetrahedron based fast 3D fingerprint identification using colored LEDs illumination," *IEEE Trans. Pattern Anal. Mach. Intell.*, vol. 40, no. 12, pp. 3022–3033, Dec. 2018.
[69] C. Lin and A. Kumar, "Matching contactless and contact-based conventional fingerprint images for biometrics identification," *IEEE Trans. Image Process.*, vol. 27, no. 4, pp. 2008–2021, Apr. 2018.
[70] A. Kumar and Y. Zhou, "Contactless fingerprint identification using level zero features," in *Proc. Comput. Vis. Pattern Recognit. Workshops*, 2011, pp. 114–119.
[71] "Image analysis & biometrics lab fingerprint database," Accessed: Sep. 2023. [Online]. Available: https://iab-rubric.org/resources/biometric-datasets/fingerprint
[72] A. Malhotra, S. Chhabra, M. Vatsa, and R. Singh, "On privacy preserving anonymization of finger-selfies," in *Proc. IEEE/CVF Conf. Comput. Vis. Pattern Recognit. Workshops*, 2020, pp. 120–128.
[73] A. Sankaran, M. Vatsa, and R. Singh, "Multisensor optical and latent fingerprint database," *IEEE Access*, vol. 3, pp. 653–665, 2015.
[74] Y. I. Shehu et al., "Sokoto coventry fingerprint dataset," 2018, *arXiv.1807.10609*.
[75] B. Jawade, D. D. Mohan, S. Setlur, N. Ratha, and V. Govindaraju, "RidgeBase: A cross-sensor multi-finger contactless fingerprint dataset," in *Proc. IEEE Int. Joint Conf. Biometrics*, 2022, pp. 1–9.
[76] F. Liu et al., "A flexible touch-based fingerprint acquisition device and a benchmark database using optical coherence tomography," *IEEE Trans. Instrum. Meas.*, vol. 69, no. 9, pp. 6518–6529, Sep. 2020.
[77] "SZU OCT-based fingerprint database." Aug. 2019. Accessed: Jul. 2022. [Online]. Available: https://github.com/FengLiu-0013/A-Benchmark-Database-using-Optical-Coherence-Tomography-for-Fingerprints
[78] A. Ross, S. Dass, and A. Jain, "A deformable model for fingerprint matching," *Pattern Recognit.*, vol. 38, no. 1, pp. 95–103, Jan. 2005.
[79] T. Elham et al., "NIST Fingerprint Image Qual. 2," *NIST Interagency/Internal Rep.*, Nat. Inst. Standards Technol., Gaithersburg, MD, USA, Jul. 2021.
[80] "Neurotechnology, VeriFinger SDK 11.1." Mar. 2019. Accessed: Jul. 14, 2022. [Online]. Available: http://www.neurotechnology.com
[81] J. J. Engelsma, K. Cao, and A. K. Jain, "Learning a fixed-length fingerprint representation," *IEEE Trans. Pattern Anal. Mach. Intell.*, vol. 43, no. 6, pp. 1981–1997, Jun. 2021.
[82] "Anguli: Synthetic fingerprint generator," Accessed: Aug. 2023. [Online]. Available: https://dsl.cds.iisc.ac.in/projects/Anguli/
[83] J. Kittler, M. Hatef, R. P. W. Duin, and J. Matas, "On combining classifiers," *IEEE Trans. Pattern Anal. Mach. Intell.*, vol. 20, no. 3, pp. 226–239, Mar. 1998.
[84] F. Liu, G. Liu, W. Zhang, L. Wang, and L. Shen, "A novel high-resolution fingerprint representation method," *IEEE Trans. Biometrics, Behav., Identity Sci.*, vol. 4, no. 2, pp. 289–300, Apr. 2022.
[85] Q. Pang, Y. Xu, F. Chen, G. Lu, and D. Zhang, "Hierarchical pore-based high-resolution fingerprint indexing," *IEEE Trans. Instrum. Meas.*, vol. 71, 2022, Art. no. 5001213.
[86] D. R. Ashbaugh, *Quantitative-Qualitative Friction Ridge Analysis: An Introduction to Basic and Advanced Ridgeology*. Boca Raton, FL, USA: CRC Press, 1999.

[87] J. Thornton, "Latent fingerprints, setting standards in the comparison and identification," in *Proc. 84th Ann. Training Conf. California State Division IAI*. May 2000. Accessed: Jul. 2022. [Online]. Available: http://www.latent-prints.com/thornton.htm
[88] B. Ding et al., "Subcutaneous sweat pore estimation from optical coherence tomography," *Inst. Eng. Technol. Image Process.*, vol. 15, no. 13, pp. 3267–3280, May 2021.
[89] Y. Yu, H. Wang, Y. Zhang, R. Liang, and P. Chen, "Methods and applications of fingertip subcutaneous biometrics based on optical coherence tomography," *IEEE Trans. Biometrics, Behav., Identity Sci.*, vol. 5, no. 1, pp. 126–150, Jan. 2023.
[90] Y. Zhang, X. Li, H. Wang, R. Wang, P. Chen, and R. Liang, "Sweat gland extraction from optical coherence tomography using convolutional neural network," *IEEE Trans. Instrum. Meas.*, vol. 72, 2023, Art. no. 5003816.
[91] Y. Yu et al., "Optical coherence tomography in fingertip biometrics," *Opt. Lasers Eng.*, vol. 151, Apr. 2022, Art. no. 106868.
[92] L. N. Darlow, L. Webb, and N. Botha, "Automated spoof-detection for fingerprints using optical coherence tomography," *Appl. Opt.*, vol. 55, no. 13, pp. 3387–3396, Apr. 2016.
[93] H. Sun, Y. Zhang, P. Chen, H. Wang, Y.-P. Liu, and R. Liang, "A new approach in automated fingerprint presentation attack detection using optical coherence tomography," *IEEE Trans. Inf. Forensics Secur.*, vol. 18, pp. 4243–4257, 2023.
[94] T. Chugh and A. K. Jain, "OCT fingerprints: Resilience to presentation attacks," 2019, *arXiv:1908.00102*.
[95] H. Sun, Y. Zhang, P. Chen, H. Wang, and R. Liang, "Internal structure attention network for fingerprint presentation attack detection from optical coherence tomography," *IEEE Trans. Biometrics, Behav., Identity Sci.*, vol. 5, no. 4, pp. 524–537, Oct. 2023, doi: 10.1109/TBIOM.2023.3293910.
[96] Y.-P. Liu, W. Zuo, R. Liang, H. Sun, and Z. Li, "Prototype-guided autoencoder for OCT-based fingerprint presentation attack detection," *IEEE Trans. Inf. Forensics Secur.*, vol. 18, pp. 3461–3475, 2023.
[97] A. M. Jiménez, S. Grelet, V. Tsatourian, P. B. Montague, A. Bradu, and A. Podoleanu, "400 Hz volume rate swept-source optical coherence tomography at 1060 nm using a KTN deflector," *IEEE Photon. Technol. Lett.*, vol. 34, no. 23, pp. 1277–1280, Dec. 2022.
[98] C. Chen, W. Shi, and V. X. D. Yang, "Real-time en-face Gabor optical coherence tomographic angiography on human skin using CUDA GPU," *Biomed. Opt. Exp.*, vol. 11, no. 5, pp. 2794–2805, 2020.
[99] J. D. Farrell et al., "Geometrically accurate real-time volumetric visualization of the middle ear using optical coherence tomography," *Biomed. Opt. Exp.*, vol. 14, no. 7, pp. 3152–3171, 2023.
[100] B. Ding, H. Wang, R. Liang, Y. Zhang, and P. Chen, "End-to-end surface and internal fingerprint reconstruction from optical coherence tomography based on contour regression," *IEEE Trans. Inf. Forensics Secur.*, vol. 18, pp. 162–176, 2023.

Haohao Sun received the BEng and PhD degrees from the College of Information Engineering, Zhejiang University of Technology, Hangzhou, China, in 2017 and 2023, respectively. He is currently a postdoc with the College of Computer Science and Technology, Zhejiang University of Technology, China. His research interests include biometric recognition and optical imaging.

Haixia Wang (Member, IEEE) received the BS and PhD degrees in computer engineering from Nanyang Technological University, Singapore, in 2007 and 2012, respectively. She is currently a professor with the College of Computer Science and Technology, Zhejiang University of Technology, China. Her research interests include biometric image processing, pattern recognition, and 3-D measurements.

Yilong Zhang (Member, IEEE) received the PhD degree from Tsinghua University, China, in 2017. He is an assistant professor with the College of Computer Science and Technology, Zhejiang University of Technology, China. His main research interests include biomedical optical imaging and pattern recognition.

Ronghua Liang (Senior Member, IEEE) received the BS degree from Hangdian University in 1996, and the Ph.D. degree from Zhejiang University in 2003. He was a research fellow with the University of Bedfordshire, U.K., from 2004 to 2005 and as a visiting scholar with the University of California, Davis in the U.S. from 2010 to 2011. He is currently a professor with the College of Computer Science and Technology, Zhejiang University of Technology, China. His research interests include computer vision, computer graphics, and medical visualization.

Peng Chen (Member, IEEE) received the BSc and PhD degrees from Zhejiang University, Hangzhou, China, in 2003 and 2009, respectively. He was a visiting scholar with the University of California, Santa Barbara, U.S., from 2015 to 2016. He is currently a professor with the College of Computer Science and Technology, Zhejiang University of Technology, China. His main research interests include computer vision and signal processing.

Jianjiang Feng (Member, IEEE) received the BEng and PhD degrees from the School of Telecommunication Engineering, Beijing University of Posts and Telecommunications, China, in 2000 and 2007, respectively. From 2008 to 2009, he was a postdoctoral researcher with PRIP Laboratory, Michigan State University. He is currently an associate professor with the Department of Automation, Tsinghua University, Beijing. His research interests include fingerprint recognition and computer vision. He is an associate editor for *Image and Vision Computing*.